

SUMMER
UNDERGRADUATE
RESEARCH PROGRAM

2019

RESEARCH JOURNAL

UCLA Samueli
School of Engineering

Summer Undergraduate Research Program at the Engineering Student Resource Center
Office of Academic and Student Affairs
UCLA Samueli School of Engineering
420 Westwood Plaza, 6288 Boelter Hall, Los Angeles, CA, 90095-1600
310.825.9478 | www.samueli.ucla.edu



Table of Contents

Student Research Abstracts & Posters

2	Neha Adhlakha	32	Michelle Lam	62	Shantinath Smyth
4	Nathan Atkinson	34	Vincent Lau	64	Dan Song
6	Abbas Bakhshandeh	36	Brandon Le	66	Wenhui Sui
8	Pranav Balgi	38	Jifei Liu	68	Irfan Syed
10	Arhison Bharathan	40	Kajal Maran	70	Madeline Taylor
12	Jason Bustani	42	Alicia Mercado	72	Ravi Varma
14	Cindy Chang	44	Michael Molter	74	Sydney Walsh
16	Brian Chap	46	Noa Nambu	76	Hou Seng Wong
18	Sean Dao	48	Marcel Nwaukwa	78	Derek Xiao
20	Gustavo Diaz	50	Robert Ozturk		
22	Alyssa Eckley	52	Naveene Raya		
24	Lucas He	54	Tara Sadjadpour		
26	Tz-Wei Hung	56	Rachel Schwall		
28	Tyler Kaplan	58	Justin Shao		
30	Chelsea Lai	60	Robert Shi		

Poster Symposium and Awards Ceremony | August 16, 2019

First Floor Engineering VI: Mong Auditorium, Lobby and Patio

11:00 AM - 11:05 AM Announcement (William Herrera)

11:05 AM - 12:30 PM Poster Galley Walk

11:45 AM - 12:30 PM Hors d'oeuvres service begins

12:30 PM - 2:00 PM Awards Ceremony



DEAN'S MESSAGE

The Summer Undergraduate Research Program (SURP) provides participants with an intensive 8-week summer research experience in a wide range of engineering fields. Undergraduate students participate in research with UCLA Samueli School of Engineering faculty and research teams to gain real-world lab experience. As part of this program, SURP students:

- Meet and network with peers who have similar goals and interests
- Learn to communicate research outcomes by participating in weekly Technical Presentation Labs
- Create a professional scientific poster of their research
- Write and publish a research abstract
- Present a detailed Summary of Project
- Become more competitive when applying to engineering graduate schools

This year, 39 undergraduate students were selected to join the 2019 SURP cohort. I would like to congratulate this SURP class on completion of their amazing research projects. Creating new knowledge is a very important, and a very difficult, task. These high-performing students have done an outstanding job working through the rigors and challenges of full time research. They should be very proud of the abstracts and posters they have published today. I encourage you to meet the students, ask questions about their projects, and learn about the cutting-edge knowledge that is being created here at the UCLA Samueli School of Engineering.

Sincerely,

Jayathi Murthy

Ronald and Valerie Sugar Dean



LAB NAME
Signal Processing and Circuit Engineering Laboratory

FACULTY ADVISOR
Professor Sudhakar Pamarti

GRADUATE STUDENT DAILY LAB SUPERVISOR
Shi Bu

DEPARTMENT
Electrical and Computer Engineering

Neha Adhlakha
Electrical Engineering
Second Year
UCLA

Filter Behavior Characterization and Verification Utilizing Analog to Digital Converter and Digital Signal Processing

High-performance integrated electrical filters are desired in almost every aspect and found in almost all electronic devices. In realizing very sharp and linear analog filters with enhanced wave filtering applications, our lab began utilizing an intentional use of time varying circuits. However, for such filters to be truly useful, it needs precise characterization with fast, and preferably automated processes. Developing this automation involved signal generators and an analog-to-digital converter to create a quick and precise characterization of the behavior of various filters which would otherwise be done manually which is time consuming and inefficient. The ADC board combined with two synchronized signal generators allows the signal to be sent to a MATLAB algorithm and hence obtain the desired magnitude and phase responses of the filter. The signal generation and process is more complex than sweeping the input frequency because the automation produces many challenges including equipment noise. My research aims to overcome these obstacles with digital signal processing. Our process of characterizing the parameters of a filter quickly and precisely will contribute to our labs development of a frequency-channelized ADC that will use tens of such filters to separate the spectrum into multiple pieces.

Samueli
School of Engineering

Summer Undergraduate
Research Program

Fast Track to SUCCESS
summer scholars program
Electrical Engineering Department
UCLA School of Engineering

Filter Behavior Characterization and Verification Utilizing Analog to Digital Converter and Digital Signal Processing

UCLA Department of Electrical and Computer Engineering
N. Adhlakha, A. Bakhshandeh, S. Bu, S. Pamarti

Introduction

High-performance integrated electrical filters are desired in almost every aspect and found in almost all electronic devices. In realizing very sharp and linear analog filters with enhanced wave filtering applications, our lab began utilizing an intentional use of time varying circuits. However, for such filters to be truly useful, it needs precise characterization with fast, and preferably automated processes. This automation created a quick and precise characterization of the behavior of various filters which would otherwise be done manually which is time consuming and inefficient. The techniques developed in this research used off-the-shelf filters for proof of concept and will be used to measure the fabricated LPTV-circuit-based chips so that we will build the frequency-channelized ADC.

Automation

GPIB
In order to manually automate the synchronized E4422b signal generators, we connected them with GPIB and a NI GPIB board which connects through usb to a computer. Then the signal generators are controlled by MATLAB code which sweeps the frequency of both generators by 1MHz until the algorithm is stopped.

Visual Analog
The signal data is processed through Visual Analog software, which we use for sampling and automation to extract the magnitude and phase. The data is sent through the input formatter, data router, and pattern saver which saves the data in a new txt file in a folder every 1000 ms. This allows the data to be sent through an automation algorithm to characterize the filter at each frequency.

Measurement Principles and Setup

Low Pass Filter

The setup below is used with two synchronized Signal Generators in phase which sends two signals, one at a high frequency, and one at a low frequency through a power combiner. Then the two-tone signal is passed through the low pass filter and into the ADC for data collecting and sent through a MATLAB algorithm.

Phase

The use of a power combiner in the setup above allowed the relative phases between an input signal 12 MHz) and a synchronized (1 MHz) signal to be represented on the graph to the left. The calculated phase of a signal in itself is irrelevant; its relative phase to an accompanying synchronized signal is used due to the fact that at the low frequencies, the filter adds negligible delay.

Amplitude

The amplitude of the signal was extracted with the use of the FFT function as well as taking the FFT processing gain into consideration. Spectrum leakage has also been taken into account. The resulting amplitude magnitude is compared to data sheets to verify the filter.

Acknowledgements

I would like to acknowledge the 2019 Summer Undergraduate Scholars Program for this amazing research opportunity, Professor Pamarti for giving us this project to contribute to his influential research, and Shi Bu our daily lab supervisor for guiding us through this project and answering all of our questions to make sure this is a huge learning experience for us.

Characterization Aspects

Challenges

- The two-tone set up is necessary because the absolute phase of one sinusoidal signal depends on when the sampling starts and is therefore useless. So, the relative phase is obtained by comparing it with a reference low-frequency signal, for which the filter has negligible delay.
- The phase of the two signal generators might be out of lock after changing the frequency which may need to be solved by using a dummy ADC setup that captures the signal prior to it passing through the filter and then compare the relative phase.

Filter Verification

To verify that the low pass filter being used worked correctly, the magnitude response was measured with a signal passing through the filter and sent through the spectrum analyzer. The results were graphed (top) and compared to the online specification (bottom), the visual drop in loss at 12 MHz verifies our filter.

Future Work and Conclusion

In conclusion, digital signal processing is a complicated task which requires many verifications of processes and obstacles to overcome with equipment use. However, the automation of characterizing filters involves synchronized Signal Generators, ADC Boards, Visual Analog Software, and a MATLAB algorithm. In the end we are able to fully characterize a filters magnitude and phase and graph the results in order to understand their precise response.

Our process of characterizing the parameters of a filter quickly and precisely will contribute to our labs development of a frequency-channelized ADC that will use tens of integrated LPTV-circuit-based filters to separate the spectrum into multiple pieces. The filters are one of the sharpest integrated filters to date and the ability to use multiple filters and characterize them precisely and accurately will allow development for advanced technology.



Nathan Atkinson
Computer Engineering
Third Year
UCLA

LAB NAME
**Terahertz Devices and Intersubband Nanostructures
Group Laboratory**

FACULTY ADVISOR
Professor Ben Williams

GRADUATE STUDENT DAILY LAB SUPERVISOR
Parastou Mortazavian

DEPARTMENT
Electrical and Computer Engineering

Diamond as an output coupler for chip-scale terahertz external cavity quantum cascade lasers

External cavity quantum cascade lasers are an integral source of terahertz radiation. However, heat removal from the devices is critical in order to achieve continuous wave operation. We introduce a chip-scale output coupler for a quantum cascade vertical external-cavity surface emitting laser (QC-VECSEL) through a 500 μm thick synthetic polycrystalline diamond plate. This design brings two primary benefits: a method of dissipating heat from the laser's bias region and a mechanically stable output coupler with no need for alignment. The diamond is mounted directly on top of the metasurface, replacing an existing design involving an externally mounted quartz output coupler. Initial electromagnetic simulations indicate acceptably high reflectance at a resonant lasing frequency of 3.4 THz and a bandwidth of about 140 GHz. Thermal simulations will be conducted to predict the expected improvements to operating temperature and heat dissipation for the VECSEL's metasurface. Possible areas of concern include high threshold current and increased thermal losses due to an adjusted ridge geometry that features a high fill factor.



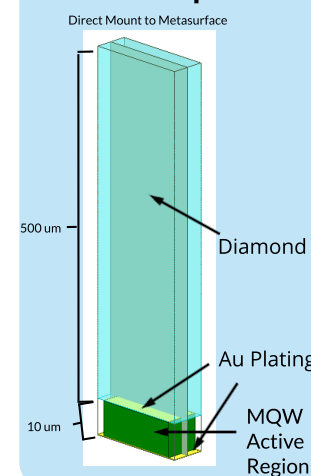
Diamond as a chip-scale output coupler for terahertz quantum cascade lasers

Nathan Atkinson, Parastou Mortazavian, Christopher Curwen, and Benjamin Williams
Department of Electrical and Computer Engineering, University of California, Los Angeles

Abstract

External cavity quantum cascade lasers are an integral source of terahertz radiation. However, heat removal from the devices is critical in order to achieve continuous wave operation. We introduce a chip-scale output coupler for a quantum cascade vertical external-cavity surface emitting laser (QC-VECSEL) through a 500 μm thick synthetic polycrystalline diamond plate. This design brings two primary benefits: a method of dissipating heat from the laser's bias region and a mechanically stable output coupler with no need for alignment. The diamond is mounted directly on top of the metasurface, replacing an existing design involving an externally mounted quartz output coupler. Initial electromagnetic simulations indicate acceptably high reflectance at a resonant lasing frequency of 3.4 THz and a bandwidth of about 140 GHz. Thermal simulations will be conducted to predict the expected improvements to operating temperature and heat dissipation for the VECSEL's metasurface. Possible areas of concern include high threshold current and increased thermal losses due to an adjusted ridge geometry that features a high fill factor.

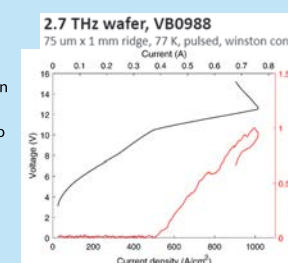
VECSEL Coupled with Diamond



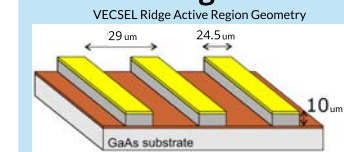
Diamond is a superb thermal conductor and a strong electrical insulator. Consequently, it serves as a viable output coupler and heat spreader for the metasurface. Placing diamond on top of the metasurface serves to remove the external cavity and create a pseudo-monolithic system which may offer improved mechanical stability in applied settings. The diamond introduces a lossy medium through which the laser beam must travel. Carbon vapor deposition (CVD) diamond has been observed to have an optical refractive index of about 2.378.² This changes the beam's resonant frequency; the ridge geometry must be adjusted to realign the resonance with the target 3.4 THz. As such, this design features a much shorter ridge gap than previous VECSELS.

Candidate Active Region

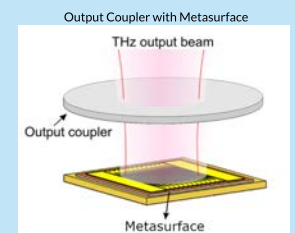
The VECSEL will be fabricated on an existing wafer design (VB0988) which has a maximum current density of about 1000 A/cm^2 . Given a fill factor of 84.5%, the nominal bias region diameter was chosen to be 1 mm. This implies a peak current of 6.6 A. Possible areas of concern moving forward primarily involve thermal performance. 500 μm thick diamond may not adequately dissipate heat from the bias region.



VECSEL Design

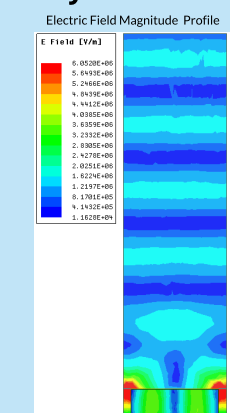
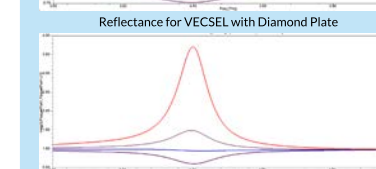
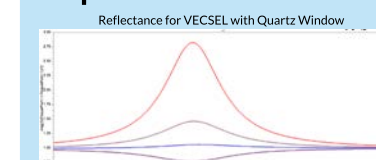


- Designed metasurface is a periodic array of coupled metal-metal ridges
- Chip-scale ridges consist of a layered multiple quantum well (MQW) semiconductor structure
- Laser cavity comprised of metasurface and a partially reflective output coupler
- Width and distance between ridges on the metasurface determine the resonant frequency, as does the distance of the output coupler from the metasurface



- Previous output coupler made of quartz
- Vacuum cavity separates metasurface and output coupler
- 3.4 THz is a standard frequency for which the VECSELS are designed¹

Response at Resonant Frequency



- Simulated reflectance maintains similar values from previous design
- Expected peak reflectance at resonant frequency (3.4 THz)
- Full-width half max bandwidth is 140 GHz at 40 cm^{-1} gain
- Free spectral range (FSR) is 126 GHz; single mode lasing expected

In electromagnetic simulations, the electric field profile appears uniform with no indication of diffraction. The high intensity patterns located periodically between ridges suggests that the device will behave similarly to a distributed feedback laser (DFB). A radiative pattern indicative of wave propagation in the normal direction is observed.

Acknowledgments

We would like to thank the National Science Foundation and the UCLA HSEAS Summer Undergraduate Research Program for providing funding for and the opportunity to publish our research, as well as the UCLA Electrical Engineering Fast Track to Success Program for its continued support of undergraduate research and studies.

References

1. Xu, L., et al. "Metasurface external cavity laser." *Applied Physics Letters*, **107**, (2015).
2. Kubarev, V., et al. "Optical properties of CVD-diamond in terahertz and infrared ranges." *Nuclear Instruments and Methods in Physics Research A*, **603**, (2009).



LAB NAME
Signal Processing and Circuit Engineering Laboratory

FACULTY ADVISOR
Professor Sudhakar Pamarti

GRADUATE STUDENT DAILY LAB SUPERVISOR
Shi Bu

DEPARTMENT
Electrical and Computer Engineering

Abbas Bakhshandeh
Electrical Engineering
Second Year
UCLA

Filter Behavior Verification and Characterization Utilizing Analog to Digital Converter and Digital Signal Processing

Electronic filters are utilized almost everywhere. However, while integrated filters are demanded in modern high-complexity systems, for them to be truly useful, we need to fully characterize them with great precision. While such characterization and testing may appear to be straightforward, many difficulties arise in practice. For example, such characterization needs to be fast and accurate, with multiple aspects being measured simultaneously. Measurement equipment non-idealities, such as noise and non-linearity, had to have been addressed with careful consideration. Our utilization of an Analog to Digital Converter (ADC) enabled an automated process with high precision, as the ADC's output could be processed digitally for better handling of various error sources. Our use of an ADC in addition to signal generators and MATLAB algorithms allowed us to automate the process of verifying the veracity of a filter's intended behavior; this process allowed us to extract properties such as magnitude and phase, some of the most important parameters to our interest. These now characterized filters can be utilized in more complex integrated systems for various communication applications. For example, the aid from the automated, precise characterization of filters will allow the building of a hybrid filter bank - which would consist of tens of filters - to achieve signal reconstruction with much less difficulty, which is key to realizing a wideband frequency-channelized ADC for high-dynamic-range and low-power applications.

Filter Behavior Verification and Characterization Utilizing Analog to Digital Converter and Digital Signal Processing



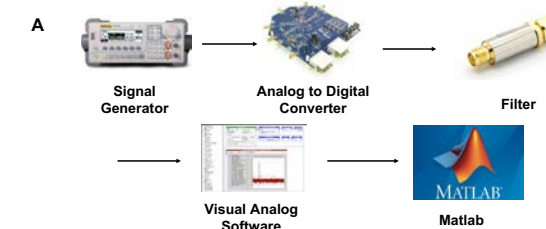
Abbas Bakhshandeh, Neha Adhalaka, Shi Bu, Sudhakar Pamarti
Department of Electrical and Computer Engineering, University of California - Los Angeles



Introduction

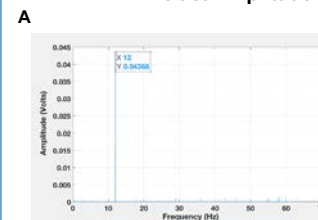
High-performance integrated electronic filters are desired in almost every aspect and found in almost all electronic devices. It is desirable to know their responses, and in some applications, it is preferable that precise measurements of the filter's frequency responses be measured. Without this step, there will be performance degradation. The utilization of the ADC enabled an automated process with high precision, as the ADC's output could be processed digitally for better handling of various error sources. Our use of an Analog to Digital Converter (ADC) in addition to signal generators and Matlab algorithms allowed us to automate the process of verifying the veracity of a filter's intended behavior; this process allowed us to extract properties such as magnitude and phase, some of the most important parameters to our interest. In our specific case, we intend to use such measurements to create a hybrid filter bank that utilizes alias cancellation. This filter bank will allow for high-dynamic range and low-power applications.

Filter Verification Setup and Process



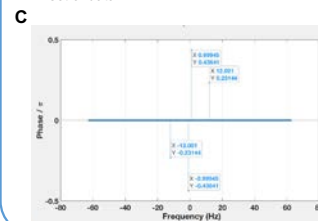
(A) The signal generator - or multiple signal generators in sync with one another to produce multiple signals - constructs a signal which is sent to the analog digital converter, which in turn passes through the filter on its way to the Visual Analog Software. The data set produced through this software is extracted, and then sent to Matlab for analysis. Within Matlab, Fast Fourier Transforms in addition to various other functions are utilized to extract the amplitude and relative phase of the signal, from which the filter's properties can be characterized and confirmed.

Utilization of Matlab Algorithms and Power Combiner to Extract Amplitude and Relative Phase



(A) The amplitude of the signal was extracted with the use of the fft function as well as taking the FFT processing gain into consideration. Spectral leakage has also been taken into account. The resulting amplitude magnitude is compared to data sheets to verify the filter's frequency response.

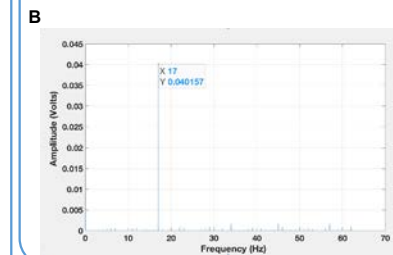
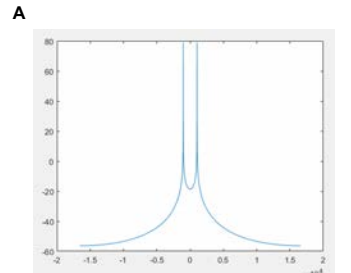
(B) The Power Combiner uses two input ports to combine two input signals into a single output signal. This is necessary in the case of analyzing the phase of a signal, as the relative phase of one signal to another is what is really desired. The power combiner allows both signals to be graphed and analyzed within one set of data.



(C) The use of a power combiner allowed the relative phases between an input signal (12 MHz in this case) and a synchronized (1 MHz) signal to be represented within one graph. The calculated phase of a signal in itself is irrelevant; its relative phase to an accompanying synchronized signal reveals its true behavior and allowed the filter to be fully characterized. This is based on the notion that at low frequencies, the filter adds negligible delay.

Spectral Leakage

(A) Whenever the period of time being analyzed does not contain an integer number of periods, spectral leakage occurs. While performing a Fast Fourier Transform, this leakage causes sharp junctions, which in turn increase the perceived frequency content of the signal. This must be accounted for in order to extract the correct relative phase value of the signal, and hence to characterize the filter effectively. This is possible to do since we know the signal frequency, which we chose as the input.



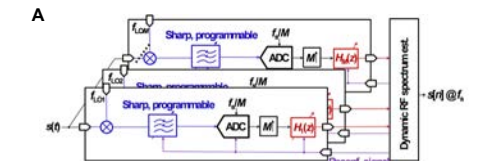
(B) To solve the issue of spectrum leakage, we are truncating the sequence such that it has an integer number of periods. This will make the sample being analyzed a better representation of the original signal. This is necessary because the FFT function assumes the data being analyzed can be reconstructed exactly as the input signal. The process of windowing, which includes the use of weighting functions, can solve this issue.

Lock-In Amplifier

$$U_{out}(t) = \frac{1}{T} \int_{t-T}^t \sin[2\pi f_{ref} \cdot s + \varphi] U_{in}(s) ds$$

(A) The methods associated with a lock in amplifier must be utilized in order to decrease the noise surrounding the signal. This is important because at frequencies where the filter greatly attenuates the signal, the input to the ADC will be too small, which will cause it to be overwhelmed by noise. Therefore, we need a lock-in amplifier to de-noise it to get the signal. The properties of a lock in amplifier were simulated in Matlab by multiplying and then integrating the data set by a reference signal of the same frequency to eliminate the effects of all frequencies not of importance.

Conclusions and Future Work



(A) Looking forward, the algorithms developed will allow for the accurate verification and characterization of the self made filters in the lab. These verified filters can be utilized in more complex integrated systems for various communication applications. A filter bank can now be constructed which will facilitate more efficient signal reconstruction; this in turn will be useful in realizing high-dynamic range and low-power applications. Additionally, our process of characterizing the parameters of a filter quickly and precisely will contribute to our labs development of a frequency-channelized ADC that will use tens of integrated LPTV-circuit-based filters to separate the spectrum into multiple pieces.

Acknowledgments

This work was supported by the Fast Track to Success Summer Scholars Program. It has also been supported and much gratitude is given to Professor Pamarti as well as Shi Bu, our daily lab supervisor, for their input on the project. Abbas Bakhshandeh is participating in the Summer Undergraduate Scholars Program at the Henry Samueli School of Engineering at UCLA.



LAB NAME
Algorithmic Research in Network Information Flow Laboratory

FACULTY ADVISOR
Professor Christina Fragouli

GRADUATE STUDENT DAILY LAB SUPERVISOR
Yahya Ezzeldin

DEPARTMENT
Electrical and Computer Engineering

Pranav Balgi
 Computer Engineering
 Third Year
 UCLA

Rodent Path Reconstruction using Hippocampal Rate Coding

The goal of this project is to use neural spike readings from a rat to determine its position in an enclosure. The spike readings are taken from several neurons in the hippocampus, a part of the brain that is associated with spatial memory. The spike readings are condensed into spike rates for each neuron, which are believed to hold information about the stimulus (the rat's position). The spike rate of each neuron is modeled as a Poisson process with an unknown parameter that is a function of the stimulus. A neural network is used to determine the parameter for every neuron at every position in the enclosure. Different sets of features from the stimulus can be used as the input to the neural network. The parameters and spike rate data are then fed into a decoder to reconstruct the original path. There are many different feature extractions, neural network architectures, and decoding schemes that can be used in this framework. The goal is to select the features, design the neural network, and build the decoder that will minimize error in the reconstructed path. Some of the decoding algorithms that have been explored in this project include one-shot decoding, greedy decoding, Viterbi decoding, and adaptive decoding. A high-performance decoder could possibly be adapted to improve brain-machine interfaces.

UCLA Samueli School of Engineering
 Summer Undergraduate Research Program

Rodent Path Reconstruction using Hippocampal Rate Coding

Pranav Balgi, Yahya Ezzeldin, Christina Fragouli
 Algorithmic Research on Networked Information Flow (ARNI)
 Department of Electrical and Computer Engineering, University of California, Los Angeles

Introduction

Goal: use neural spike readings* from a rat to determine its position in an enclosure

- spike readings are taken from multiple neurons in the rat's hippocampus
- hippocampus is a part of the brain that is associated with spatial memory
- spike readings are condensed into spike rates for each neuron,
- spike rates are believed to hold information about the stimulus (the rat's position)
- a high-performance decoder could possibly be adapted to improve decoding of neural responses which is a key interest for brain-machine interfaces

*data was provided by the W. M. Keck Center for Neurophysics at UCLA

Neural Encoding

- spike rate of each neuron (N=73) is modeled as a Poisson process
- Poisson parameters are functions of the stimulus
- different sets of features from the stimulus can be used as the input to the model
- model is trained to determine the parameter for every neuron at every position in the enclosure
- a neural network can be used for feature extraction

Path Decoding

stimuli (positions)

measured spike rates

$y_0, y_1, y_2, y_3, \dots, y_{N-1}$

log-likelihoods

$\mathcal{L}_0, \mathcal{L}_1, \mathcal{L}_2, \mathcal{L}_3, \dots, \mathcal{L}_{N-1}$

decoded path

- position is discretized by even sampling
- $\lambda_n^{(i)}$: Poisson parameter of neuron n at position i
- $y_n^{(t)}$: spike rate of neuron n at time t
- $\mathcal{L}(i | t)$: log-likelihood of being on position i at time t

$$\mathcal{L}(i | t) = \sum_{n=0}^{N-1} y_n^{(t)} \log \lambda_n^{(i)} - \lambda_n^{(i)}$$

Decoding Methods

One-Shot Decoder

- selects position with maximum likelihood at each time
- $s(t)$: decoded position at time t

$$s(t) = \underset{i}{\operatorname{argmax}} \mathcal{L}(i | t)$$

Greedy Decoder

- selects position that is within a fixed distance r of the previous position
- $s(t)$: decoded position at time t

$$s(t) = \underset{i}{\operatorname{argmax}} \mathcal{L}(i | t) \text{ s.t. } \|p(i) - p(s(t-1))\| \leq r$$

Viterbi Decoder

- selects path with maximum likelihood out of all possible paths
- $s(i, t)$: maximum likelihood previous position from position i at time t
- $m(i, t)$: path metric on position i at time t

$$s(i, t) = \underset{j}{\operatorname{argmax}} m(j, t-1) + \mathcal{L}(i | t) \text{ s.t. } \|p(i) - p(j)\| \leq r$$

$$m(i, t) = \mathcal{L}(s(i, t) | t-1) + \mathcal{L}(i | t)$$

Adaptive Decoding

- selects position that is within a variable distance r of the previous position
- r is proportional to current speed

$$s(t) = \underset{i}{\operatorname{argmax}} \mathcal{L}(i | t)$$

$$\text{s.t. } \|p(i) - p(s(t-1))\| \leq \alpha \|p(s(t-1)) - p(s(t-2))\|$$

Results

- Viterbi decoding performs the best, but at the cost of running time
- adaptive decoding slightly improves the greedy decoder, but not the Viterbi decoder
- performance decreases as the testing interval moves away from the training interval
- decoders perform better when trained on future intervals rather than past intervals
- all of these decoders can run in real time, with the Viterbi decoders requiring a delay
- one-shot decoding performs the worst, showing that more sophisticated decoding algorithms can improve performance

Future Work

- explore more decoding algorithms
- try out different neural network architectures for encoding
- try out new feature extractions for encoding
- select different combinations of neurons to use



LAB NAME
Terahertz Electronics Laboratory

FACULTY ADVISOR
Professor Mona Jarrahi

GRADUATE STUDENT DAILY LAB SUPERVISOR
Dr. Nezhil Yardimci and Dean Turan

DEPARTMENT
Electrical and Computer Engineering

Arhison Bharathan
 Electrical Engineering
 Second Year
 UCLA

A High-Speed, Low-Cost, and Compact Optical Delay Stage for Terahertz Time-Domain Spectroscopy Systems

Terahertz Time-Domain Spectroscopy (THz-TDS) is an application of the terahertz band of the electromagnetic spectrum with advanced capabilities in chemical identification, material characterization, and nondestructive material analysis. Recent developments in THz emitter and detector technology have established improved signal-to-noise ratios within these systems, increasing the viability of THz-TDS in commercial applications. However, the weight and speed of these systems are also limited by a component known as the delay stage, a mechanical device used to vary laser optical path length. The focus of our research has been to create a miniaturized, high-speed delay stage to address this need.

While laboratory delay stages offer sub-micron accuracies, these systems are often large and expensive due to the extra functionality they provide. We have opted to explore alternative mechanisms to achieve compact and cost-effective designs that suit our application. Utilizing 3D printing and machining, we have created prototype stages using crank and crank-inspired mechanisms that achieve reciprocation frequencies of 10.4 Hz (as compared to 1.2 Hz by a laboratory stage). Through comparisons of THz-TDS results between a laboratory stage and our stages in the clarity and accuracy of absorbed THz waves measured through air, we have also been able to classify the efficacy of each iteration of our device. Looking at areas other than performance, our stages are lighter (211 g to 17 kg) and cheaper (about \$200 to \$10k) as well.

A High-Speed, Low-Cost, and Compact Optical Delay Stage for Terahertz Time-Domain Spectroscopy Systems



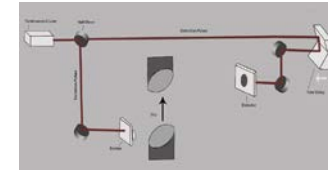
Arhison Bharathan, Madeline Taylor, Nezhil Yardimci, Deniz Turan, Mona Jarrahi
 Department of Electrical and Computer Engineering, University of California – Los Angeles



UCLA Samueli School of Engineering
 Summer Undergraduate Research Program

Background – What is THz-TDS?

Terahertz Time-Domain Spectroscopy (THz-TDS) is a well-established technology within the field of terahertz (THz) research. Created in the early 90's, this technology exploits the electromagnetic absorption properties of matter in the THz waveband for purposes of chemical identification, material characterization, and nondestructive material analysis.



THz-TDS System Operation:

- THz emitter - receives a femtosecond IR pulse and emits THz radiation towards sample
- THz detector - upon receiving a femtosecond IR pulse and THz pulse, acts as a switch to allow current pass when struck simultaneously
- Delay Stage - moves two mirrors at 90° on a carriage to vary the optical path length of the IR pulse to the detector. This allows for time-domain reconstruction of the pulse (see Figure 1). A Fourier transform of this reconstruction yields the frequency-domain characteristics of the pulse (see Figure 2).

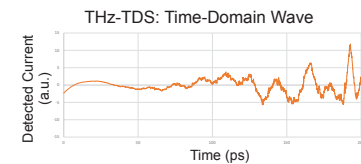


Figure 1 – Reconstructed THz wave through air using a laboratory delay stage

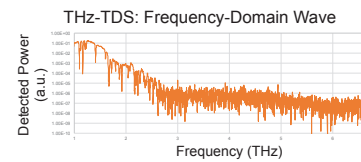


Figure 2 – Fourier transform of Figure 1 from which absorbed THz frequencies can be determined

Objective

Recent technological advancements in THz-TDS systems—due to the creation of more powerful sources and more sensitive emitters which offer better signal-to-noise ratios—have made the use of this technology practical at a commercial scale. To optimize the size and speed of such systems, another necessity is to create a compact, high-speed delay stage to increase system portability and usability. Our research objective is to develop this miniaturized delay stage. By leveraging speed, cost, and size, we aim to create a delay stage at a size suitable for commercial use. To gauge the progress of our designs, we compare the THz wave detection results from our stage and a laboratory delay stage, looking the clarity and accuracy of absorbed frequencies. Other statistics like travel, weight, and size are also considered.

Crank Mechanism - Proof of Concept

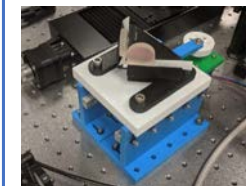
We have chosen to use a crank mechanism to drive our stage since it trivially achieves smooth, consistent, reciprocating linear motion. Unlike a laboratory stage, the path a crank mechanism follows is invariably so a trivial h-bridge motor controller suffices to actuate the mechanism. A lab scale prototype of this mechanism allows us to compare THz measurements between a laboratory stage and crank actuated stage to determine the viability of this mechanism for this THz-TDS.



Laboratory Stage – Newport Motorized Linear Stage IMS300LM-S

Produces accurate and precise motion at the expense of size, cost, and, speed. This stage is only practical in a laboratory setting.

Frequency	1.2 Hz
Total Travel	30 cm
Weight	17 kg
Size	55.6 cm x 18 cm x 8.9 cm
Price	about \$10,000

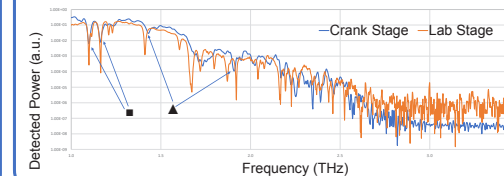


Laboratory Scale Crank Stage

This is a prototype to find out whether a crank mechanism can provide any THz-TDS measurements at all. This stage is 3D printed and uses linear slides and a stepper motor to drive the carriage.

Frequency	2.2 Hz
Total Travel	2 cm
Weight	861 g
Size	18 cm x 12.2 cm x 8.9 cm
Price	about \$150

THz Wave Absorption Through Air (Frequency-Domain) Results



- Crank Stage exhibits:
- Shallow absorption lines (■)
 - Shifted absorption lines (▲)

We believe these errors are systematic nature. Since we can account for such errors through post-processing, we conclude that a crank mechanism shows promise in a THz-TDS system.

Current Work – Mechanism Miniaturization

We use an iterative design approach to create smaller, high-speed versions of the crank mechanism we previously tested. To improve precision we employ stereolithography printing and CNC routing to create the stage and actuate the carriage on linear bearings on shafts.

High speed DC motor increases max reciprocation frequency

Low rotational inertia flywheel results in poor frequency stability

Crank-inspired eccentric reduces vibration and improves frequency stability due to high rotational inertia

Dual linear bearings per rail improve vertical beam precision

Stage	A	B	C
Frequency (Hz)	N/A ¹	10.4	N/A ²
Total Travel (cm)	1.2	0.7	1.1
Weight (g)	101	211	N/A ²
Size (cm ³)	7.4 x 6.6 x 4.6	9.4 x 6.2 x 5.4	
Price	\$220	\$260	\$300

¹. Frequency instability makes this value nonessential
². N/A statistics have not been measured due to work in progress

Conclusion and Future Work

A crank mechanism presents promising results for use in the actuation of a THz-TDS delay stage. Once our stage is mechanically complete, we plan to develop a motor control scheme utilizing position feedback to further improve frequency stability. Utilizing superior manufacturing techniques (e.g. CNC machining) will also contribute to stage precision and speed.

Acknowledgments:

- UCLA Summer Undergraduate Research Program (SURP)
- Terahertz Laser Lab
- Mona Jarrahi, Nezhil Yardimci, Deniz Turan
- UCLA Rieber Makerspace



LAB NAME
Terahertz Devices and Intersubband Nanostructures Laboratory

FACULTY ADVISOR
Professor Benjamin Williams

GRADUATE STUDENT DAILY LAB SUPERVISOR
Anthony Kim

DEPARTMENT
Electrical and Computer Engineering

Cindy Chang
 Electrical Engineering
 Second Year
 UCLA

Analyzing and Quantifying Laser Beam Quality Using the Knife Edge Technique to Calculate the M^2 Factor

A laser's beam quality is a critical parameter in the performance of the laser in the laboratory or for industrial use. Describing the beam quality entails measuring the beam's spot size, a fundamental problem in laser diagnostics as laser beams are often irregular in shape. This is due to the various modes in a laser beam. The ideal Gaussian beam consists of the fundamental lowest-order TEM₀₀ mode and has an irradiance beam profile described by a Gaussian function. We demonstrate a beam quality factor measurement of a terahertz quantum-cascade vertical external cavity surface-emitting laser (QC-VECSEL). The external cavity ideally allows for lasing at the fundamental Gaussian mode. Using a knife-edge measurement scheme, the M^2 factor can be extracted, which describes the extent to which the beam is diffraction limited.

The knife edge technique uses a converging lens to focus on the beam and makes a series of stepped measurements with a knife-edge in two different transverse directions at and around the lens's focus where the beam radius is minimized. This allows the calculation of the beam's spot size, the radius of the beam containing the majority of the power, by measuring the transmitted power with the shift of the knife in the transverse directions. By analyzing the behavior of the beam radius across the optic axis, the divergence of the beam is characterized.

UCLA Samueli School of Engineering

Analyzing and Quantifying Laser Beam Quality Using the Knife Edge Technique to Calculate the M^2 Factor

Cindy Chang, Anthony Kim, and Professor Benjamin Williams

Introduction

A laser beam is created by photons bouncing between two mirrors. The longitudinal mode determines the frequency, wavelength, and thus color of the beam. The transverse modes are described by the distribution of the irradiance along the radial direction. An ideal laser beam only consists of the fundamental lowest-order TEM₀₀ mode and has an irradiance beam profile described by a Gaussian function; however, real lasers are not ideal and typically oscillate in the lowest and possibly higher-order modes. To quantify the beam quality of a laser, the knife edge technique takes the waist measurements from stepping a knife incrementally through a beam. The MATLAB curve fitting calculates the M^2 factor in the transverse directions.

Apparatus

Terahertz Laser

Terahertz laser or far-infrared laser is a laser with an output wavelength in the far infrared, terahertz frequency band of the electromagnetic spectrum between 30-1000 μm . The laser used in this experiment is the quantum-cascade (QC) vertical-external-cavity surface-emitting-laser (VECSEL). The metasurface acts as an amplifying mirror in the external cavity allowing for an increased beam quality. The experiment's specific laser operates with 1.7 mW average power, pulsed mode, 10% duty cycle at 3.44 THz, 77K operating temperature.

Methods

With the labview program, the knife edge makes stepped movements in the transverse directions, taking and storing the detector's irradiance measurements in a textfile along with the x, y, and z positions of the knife. The apparatus holding the knife is then moved to a different location along the z axis. The program pauses until the user indicates that the knife is in position for another set of measurements and the program loops again for the transverse directions in the new z position. To ensure the program made at least five measurements within one Rayleigh length and at least five outside, the z measurements spanned several millimeters with the step size determined from the Rayleigh length. The error function was fitted to wash out drastic effects of diffraction. The 10-90% criteria for the beam waist was then used to determine waist measurements. This 10-90% criteria was chosen because of the clip levels rationalized using variances in the transverse directions³. It defined the waist size as the width where 10-90% of the total irradiance was measured. Curve fitting was then used to find the equation of the hyperbola that most accurately described our experimental data. This provided the value of beam waist constant, w_0 , which was then used in our M^2 calculations for the transverse directions.

$$w_x^2(x) = w_{0x}^2 \left[1 + \left(\frac{x - z_{0x}}{z_{Rx}} \right)^2 \right]$$

$$z_{0x} = z \text{ offset}$$

$$z_{Rx} = \frac{\pi w_{0x}^2}{\lambda}$$

$$w_x^2(x) = w_{0x}^2 + M_x^2 \left(\frac{\lambda}{\pi w_{0x}} \right)^2 (x - z_{0x})^2$$

Future Work

The small M^2 values were most likely due to diffraction effects from the experimental set up and the knife edge effects. Several mirrors were used to reflect the beam before detecting the irradiance. Altering the experimental set up to limit these diffraction effects in future work will make the experiment and results more accurate. The experimental setup also had to take into account that while the x and y movements were motorized, the z steps had to be done manually, significantly slowing down the data acquisition process. Using a motor to turn the z position would aid in future M^2 calculations. Additionally, making the labview programmatically calibrate the start and final z positions will make the experiment notably more efficient.

Results

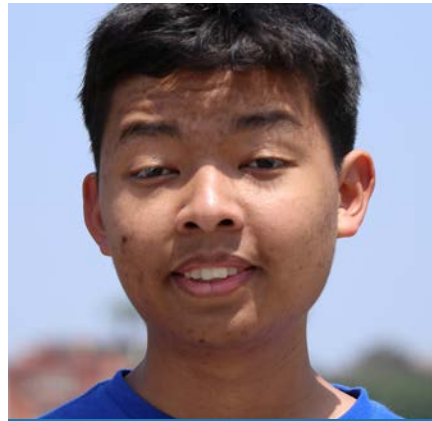
The beam waist for the x and y directions were 0.17 mm and 0.20 mm respectively, as shown by Figures 10 and 11. The M_x^2 and M_y^2 values were calculated as 1.12 and .8612 respectively. The obtained value being under unity implies that there were errors in the measurement. This discrepancy was most likely due to diffraction effects during the knife-edge measurements. Optical responses involved in the diffraction at metal edges are dependent on the laser's polarization⁴. This laser used was horizontally linearly polarized, resulting in different diffraction behaviors between the two transverse directions. Orienting the knife at a 45 degree angle to the polarization may have suppressed these differences. Figure 12 shows these effects in the integrated intensity data before the fitting. The small peaks in the plot indicate disturbances in the optical alignment due to the knife-edge diffraction. This will ultimately influence our final results.

References

- [1] Siegman, A. E. "Defining, measuring, and optimizing laser beam quality." Proc. SPIE 1868, *Laser Resonators and Coherent Optics: Modeling, Technology, and Applications*, 13 August 1993.
- [2] Siegman, A. E. "How to (Maybe) Measure Laser Beam Quality." *IPSS (Diode Pumped Solid State) Lasers: Applications and Issues*, 1998.
- [3] Siegman, A. E., et al. "Choice of Clip Levels for Beam Width Measurements Using Knife-Edge Techniques." *IEEE Journal of Quantum Electronics*, vol. 27, no. 4, 1991, pp. 1098-1104.
- [4] Suzuki, Kenta, et al. "Spatio-Temporal Imaging of Terahertz Electric-Field Vectors: Observation of Polarization-Dependent Knife-Edge Diffraction." *Applied Physics Express*, vol. 12, no. 5, 2019, p. 052010. doi:10.7577/apex.19050512c.

<https://www.orcnl.gov/arc/arc-research/terahertz-imaging/>
https://www.researchgate.net/publication/331705048/Laser_Beam_Measurements_using_Knife-Edge_Technique
<https://doi.org/10.1364/ol.19910511>

We would like to thank the National Science Foundation for providing funding for our undergraduate research. We would also like to extend our thanks to the UCLA Electrical Engineering Fast Track to Success Program and UCLA Samueli Engineering SURP for its continued and valued support in research and academic studies.



LAB NAME
UCLA Visual Machines Group Laboratory

FACULTY ADVISOR
Professor Achuta Kadambi

GRADUATE STUDENT DAILY LAB SUPERVISOR
Guangyuan Zhao

DEPARTMENT
Electrical and Computer Engineering

Brian Chap
Electrical Engineering
First Year
UCLA

Implementing Kinematic Prediction via Physics-Guided Neural Networks

Physics-guided neural networks (PGNNs) are crucial for modeling resistive behaviors in real-life scenarios ranging from vehicle tracking to aerial trajectories. In prior papers, bounding box construction for videos would entail construction for every individual frame, hindering progress in terms of speed-up without significant computational power. This paper aims to bridge the divide between image and video object detection, utilizing kinematic priors to predict the motion of subjects via the incorporation of affine transformations and perspective consideration (horizon, side-to-side, overhead, etc.). Approaches based on optical flow algorithms and tubelet architectures are considered, and blended with physical modules to harness spatiotemporal coherence among individual frames. PyTorch 1.0 acts as the framework for code development, and all code is expected to be open-source for future development.

Functional Nanomaterials
UCLA ENGINEERING
Summer Scholars Program

UCLA Samueli School of Engineering
Summer Undergraduate Research Program

Implementing Kinematic Prediction via Physics-Guided Neural Networks

Brian Chap, Lucas He, Irfan Syed
Guangyuan Zhao, Achuta Kadambi
Department of Electrical and Computer Engineering, UCLA

Visual Machines
NSF
Fast Track to SUCCESS
summer scholars program
Electrical Engineering Department
Cines and Informatics Laboratories

Using Physics-Based Machine Learning to Track Objects

Physics-guided neural networks (PGNNs) are crucial for modeling resistive behaviors in real life scenarios ranging from vehicle tracking to aerial trajectories. In prior papers, bounding box construction for videos would entail construction for every individual frame, hindering progress in terms of speed without significant computational power. This paper aims to bridge the divide between image and video object detection, utilizing kinematic priors to predict the motion of subjects via the incorporation of affine transformations and perspective consideration (horizon, side-to-side, overhead, etc.). Approaches based on optical flow algorithms and tubelet architectures are considered and blended with physical modules to harness spatiotemporal coherence among individual frames. PyTorch 1.0 acts as the framework for code development and all code is expected to be open-source for future development.

Regional Convolutional Neural Networks



Figure 1 : Improvements such as clearer annotations and bounding box representations were made on a Faster R-CNN framework with 20 different classifications of objects. The physics model resulted from this framework of Faster R-CNN.

Dataset



Applications of physics-based calculations on the Faster R-CNN framework were tested on a self-made dataset of videos that captured optimal scenarios, including drops, tosses, and object sliding on surfaces to model the effects of gravity, resistance, and object motion. The added complexity of object occlusion was captured for the purpose of modeling realistic difficulties in object detection and motion prediction.

Physics-Based Model



The midpoint of a bounding box (above) was used to calculate distance

If ground truth is close to the predicted bounding box, increase confidence probabilities. If ground truth is far from the predicted bounding box, decrease confidence probabilities.

Future Plans

The proposed physics model performs with high confidence values in the ideal scenarios created within the dataset. Expectations for future improvements include higher efficiency rates, faster processing rates, greater accuracy between multiple objects, and more accurate predictions for accounted complexities such as occlusions, lighting, and camera motion.

Limitations of current model:

- Inability to account for changing acceleration
- Inability to predict object motion with occlusions
- Prediction model accounts for only 2D object transformations.
- Unidentified objects lack physics-based machine learning

Applications:

- Self-Driving
- Autonomous Drones
- Defense Industry
- Movement Prediction

Preliminary Results



0.816



0.967



0.88 0.989 0.988 0.589 0.588



0.988 0.988 0.588

Figure 4: Bottle detection without physics-based learning (left) and with physics-based learning (right)

Figure 5: Multiple object detection without physics-based learning (left) and with physics-based learning (right)

The physics-based model results indicate significant increases in the accuracy of the model when compared with simply the Faster R-CNN framework. Faster R-CNN with physics-based machine learning increases the confidence of object detection and removes classification errors for objects.

References

Saha, Sumit. A Comprehensive Guide to Convolutional Neural Networks — the EL15 Way. *Towards Data Science*, (2018).

Lei, F.-F. et al. Detection and Segmentation. *Stanford University*, (2017).

Girshick, R. Fast R-CNN. *CoRR 1504.08083* (2015).

Girshick, R., et al. Rich feature hierarchies for accurate object detection and semantic segmentation. *CoRR 1311.2524* (2013).

Ren, S., et al. Faster R-CNN: Towards Real-Time Object Detection with Region Proposal Networks. *CoRR 1506.01497* (2015).

Redmon, J., et al. You Only Look Once: Unified, Real-Time Object Detection. *CoRR 1506.02640* (2015).



LAB NAME
Visual Machine Learning Group

FACULTY ADVISOR
Professor Achuta Kadambi

GRADUATE STUDENT DAILY LAB SUPERVISOR
Guanyang Zhou

DEPARTMENT
Electrical and Computer Engineering

Lucas He
 Electrical Engineering
 First Year
 UCLA

Physics-Based Object Temporal Localization Via Video Segmentation

The field of object detection has seen much advancements over the past years, especially in videos with the implementation and improvements of architectures such as Optical Flow, Tubelets, and Temporal Action Localization. However, such methods are still limited in their speed, efficiency, and accuracy, with the current fastest method running at an average of two frames per second. Thus, we propose the usage of the Physics Guided Neural Network (PGNN) to aid this task. By specifically tailoring this to detection of cars we hope to produce a naive form of detection that can track and solve transformations (i.e. scale, sheer, and direction) of cars as they travel down a road. Using segmentation, we would then be able to establish instances of the cars as apply a physics model and determine each object's trajectory based on the previous frames of the object's path. The application of the physics model will serve to reduce the computational requirements of previous methods and allow for a more accurate prediction of an object's temporal location.

Functional Nanomaterials
 UCLA ENGINEERING
 Summer Scholars Program

Implementing Kinematic Prediction via Physics-Guided Neural Networks

Brian Chap, Lucas He, Irfan Syed
 Guanyuan Zhao, Achuta Kadambi
 Department of Electrical and Computer Engineering, UCLA

Visual Machines
 NSF
 Fast Track to SUCCESS
 summer scholars program
 Electrical Engineering Department

Using Physics-Based Machine Learning to Track Objects

Physics-guided neural networks (PGNNs) are crucial for modeling resistive behaviors in real life scenarios ranging from vehicle tracking to aerial trajectories. In prior papers, bounding box construction for videos would entail construction for every individual frame, hindering progress in terms of speed without significant computational power. This paper aims to bridge the divide between image and video object detection, utilizing kinematic priors to predict the motion of subjects via the incorporation of affine transformations and perspective consideration (horizon, side-to-side, overhead, etc.). Approaches based on optical flow algorithms and tubelet architectures are considered and blended with physical modules to harness spatiotemporal coherence among individual frames. PyTorch 1.0 acts as the framework for code development and all code is expected to be open-source for future development.

Regional Convolutional Neural Networks



Figure 1 : Improvements such as clearer annotations and bounding box representations were made on a Faster R-CNN framework with 20 different classifications of objects. The physics model resulted from this framework of Faster R-CNN.

Dataset



Applications of physics-based calculations on the Faster R-CNN framework were tested on a self-made dataset of videos that captured optimal scenarios, including drops, tosses, and object sliding on surfaces to model the effects of gravity, resistance, and object motion. The added complexity of object occlusion was captured for the purpose of modeling realistic difficulties in object detection and motion prediction.

Physics-Based Model



The midpoint of a bounding box (above) was used to calculate distance

If ground truth is close to the predicted bounding box, increase confidence probabilities. If ground truth is far from the predicted bounding box, decrease confidence probabilities.

Future Plans

The proposed physics model performs with high confidence values in the ideal scenarios created within the dataset. Expectations for future improvements include higher efficiency rates, faster processing rates, greater accuracy between multiple objects, and more accurate predictions for accounted complexities such as occlusions, lighting, and camera motion.

Limitations of current model:

- Inability to account for changing acceleration
- Inability to predict object motion with occlusions

Prediction model accounts for only 2D object transformations. Unidentified objects lack physics-based machine learning

Applications:

- Self-Driving
- Autonomous Drones
- Defense Industry
- Movement Prediction

Preliminary Results



bottle
0.816



bottle
0.967



person
0.889



person
0.988

Figure 4: Bottle detection without physics-based learning (left) and with physics-based learning (right)

Figure 5: Multiple object detection without physics-based learning (left) and with physics-based learning (right)

The physics-based model results indicate significant increases in the accuracy of the model when compared with simply the Faster R-CNN framework. Faster R-CNN with physics-based machine learning increases the confidence of object detection and removes classification errors for objects.

References

Saha, Sumit. A Comprehensive Guide to Convolutional Neural Networks — the ELIS Way. *Towards Data Science*, (2018).

Lei, F.-F. et al. Detection and Segmentation. *Stanford University*, (2017).

Girshick, R. Fast R-CNN. *CoRR 1504.08083* (2015).

Girshick, R., et al. Rich feature hierarchies for accurate object detection and semantic segmentation. *CoRR 1311.2524* (2013).

Ren, S., et al. Faster R-CNN: Towards Real-Time Object Detection with Region Proposal Networks. *CoRR 1506.01497* (2015).

Redmon, J., et al. You Only Look Once: Unified, Real-Time Object Detection. *CoRR 1506.02640* (2015).



LAB NAME
Laboratory for Embedded Machines and Ubiquitous Robots (LEMUR)

FACULTY ADVISOR
Professor Ankur Mehta

GRADUATE STUDENT DAILY LAB SUPERVISOR
Professor Ankur Mehta

DEPARTMENT
Electrical and Computer Engineering

Chelsea Lai
 Electrical Engineering
 Second Year
 UCLA

Custom Printable Robotic Boats for Early STEM Education

Robotics engages students in multiple disciplines of engineering, which is increasingly important in our technology-based society. However, existing robotics kits are mostly geared toward middle- and high- school students and either cost hundreds or thousands of dollars or have limited hands-on design capabilities. This leaves customizable robotics unaffordable to many schools, as well as neglects to introduce robots to impressionable elementary-age children. Our project focused on concurrently addressing three concerns: cost, age group, and creative potential. We developed a modifiable template for an affordable robot that students design themselves, supporting a project-based learning approach, with the goal of inspiring interest in STEM in kindergartners.

Since most robotics kits are cars, we designed a robotic boat and a web-based app, which students use to create and steer the boat. One boat is made of a flat sheet of plastic folded into a 3D structure, with basic electronics propelling the vehicle, and costs under \$40 total. In the app, powered by Robot Compiler technology, students change parameters on the boat to see the effect on the 2D printable template and 3D model of the finished boat. This focus on customization encourages iterative design and engages students firsthand in the engineering innovation process. Students have flexibility in designing their robots down to the component level, fostering a sense of ownership over their project and resulting in a more self-motivated learning experience.

LEMUR

Custom Printable Robotic Boats for Early STEM Education

Chelsea Lai, Shantinath Smyth, Dr. Ankur Mehta
 Dept. of Electrical and Computer Engineering, University of California, Los Angeles

Introduction

Problems with Existing Robotics Kits

Expensive

Middle- and high-school age group

Limited hands-on design

Our Solution

- Creating a design tool for low-cost foldable robotic boats

Educational Applications

- Students design, build, and redesign robotic boats
- Hands-on experience with cycle of scientific experimentation

Developing the Design Tool

Built prototypes of mechanically powered paddleboat design

→

Motorized boat and integrated electronics into design

→

Finalized boat template

→

Model 2D template and 3D structure on RoCo

Student Design Process

1 Design in web-based app by inputting parameters

2 Print and cut out template

3 Fold and assemble boat, Test effects of chosen parameters

Easily modify components

Results

- Iterative design process and customization allows for personalized products
- Encourages experimentation and hands-on learning approach
- Teaches gateway STEM skills and engineering/design process

Total cost: ~\$30 (Retail), ~\$15 (Bulk)

Ultra-thin Power Bank: \$13

Plastic film: <\$1

2 Continuous Rotation Servos: <\$10

NodeMCU board and Motorshield: \$6

Acknowledgements

Summer Undergraduate Research Program
 Fast Track to Success Program
 LEMUR Lab, Dr. Ankur Mehta
 Wireless Health Institute

References

[1] McLurkin, James, et al. "Using multi-robot systems for engineering education: Teaching and outreach with large numbers of an advanced, low-cost robot." *IEEE transactions on education* 56.1 (2012): 24-33.
 [2] Blumenfeld, Phyllis C., et al. "Motivating project-based learning: Sustaining the doing, supporting the learning." *Educational psychologist* 26.3-4 (1991): 369-398.
 [3] Rubenstein, Michael, et al. "AERobot: An affordable one-robot-per-student system for early robotics education." 2015 IEEE International Conference on Robotics and Automation (ICRA). IEEE, 2015.
 [4] Mondada, Francesco, et al. "The e-puck, a robot designed for education in engineering." *Proceedings of the 9th conference on autonomous robot systems and competitions*. Vol. 1. No. CONF. IPCB: Instituto Politecnico de Castelo Branco, 2009.
 [5] A.M. Mehta, J. DelPreto, B. Shaya, and D. Rus. "Cogeneration of Mechanical, Electrical, and Software Designs for Printable Robots from Structural Specifications". In: *Intelligent Robots and Systems (IROS 2014)*. Chicago, IL, Sep 2014, pp. 2892-2897.
 [6] Mehta, Ankur M., and Daniela Rus. "An end-to-end system for designing mechanical structures for print-and-fold robots." 2014 IEEE International Conference on Robotics and Automation (ICRA). IEEE, 2014.

Prices of Existing Educational Robotics Kits

Robot	Retail Cost (USD)
Thymio	189
LEGO Mindstorm 3	340
Scribbler 3	199
mBot	69
Our Boat	30



LAB NAME
Neural Computation and Engineering Laboratory

FACULTY ADVISOR
Professor Jonathan Kao

GRADUATE STUDENT DAILY LAB SUPERVISOR
Professor Jonathan Kao

DEPARTMENT
Electrical and Computer Engineering

Michelle Lam
Computer Engineering
Third Year
UCLA

Studying changes of mind in decision-making

A decision is a commitment to an action after consideration of evidence and expected outcomes. The brain deliberates on available evidence to yield an action or decision. However, during cognition, we often change our minds; standard decision-making models do not fully explain why these changes of mind occur. The purpose of this study is to develop an experiment to study changes of mind, validating work by Resulaj and colleagues. It was hypothesized that noisy evidence, in the form of a random dot motion stimulus, is accumulated over time until it reaches a criterion level, or bound. An initial decision is made once this criterion is achieved. While the trials were conducted, subjects made decisions about a noisy visual stimulus, and then they indicated their choice of direction by moving a joystick according to the direction inferred. The brain then exploited further information that either reversed or reaffirmed the initial decision made. We conclude that this study supports Resulaj's findings and theory of post-initiation processing. This study is significant to understand decisions related to gambling, social selection, and probabilistic reasoning.

Studying changes of mind in decision-making

Michelle Lam¹, Alicia Mercado², Jonathan Kao¹

¹Department of Electrical and Computer Engineering, University of California – Los Angeles
²Department of Physical Sciences and Mathematics, Mount Saint Mary's University – Los Angeles

Ideas and Principles

Motivation

- A decision is a commitment to an action after consideration of evidence and expected outcomes.
- Standard decision-making models do not fully explain why changes of mind occur during the decision-making process.
- The purpose of this study is to develop an experiment to study changes of mind, validating work by Resulaj and colleagues.
- It was hypothesized that noisy evidence, in the form of a random dot motion stimulus, is accumulated over time until it reaches a criterion level, or bound.

Random Dot Motion Stimulus

- Random dot motions (RDM) are a classic stimulus used in psychophysical and physiological studies of motion processing.
- RDM occur in binary directions and can be modified to occur at different motion coherences.
 - Right v. Left
 - Up v. Down

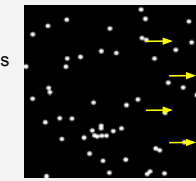


Figure 1. Random Dot Motion. Image of the random dot motion.

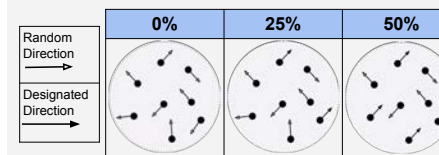


Figure 2. Motion Coherence. Motion coherence is equal to the number of dots in a designated direction divided by the number of dots total. We performed trials at motion coherences of 0%, 3.2%, 6.4%, 12.8%, 25.6%, 51.2%.

Data Collection

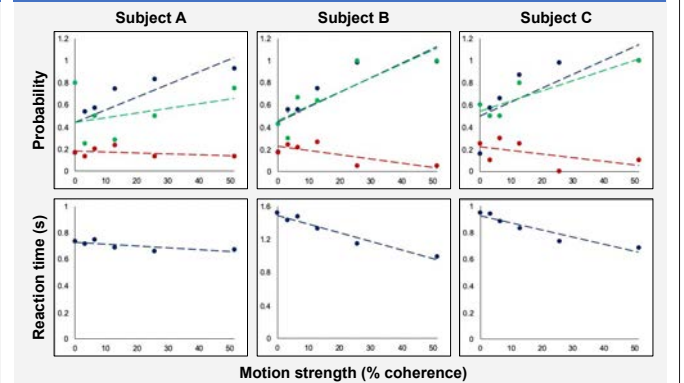


Figure 6. Accuracy improves through changes of mind. Data is from three subjects (A, B, and C). The top row shows the probability of a correct decision (blue), probability of change (red), and probability of a correct decision after change of mind (green) according to motion coherence strengths. Probability of a correct decision increases with motion strength, while probability of change decreases with motion strength. The bottom row shows that reaction times are higher for weaker motion strengths.

Conclusions

- We conclude that this study supports Resulaj's findings and theory of post-initiation processing.
- This study is significant to understand decisions related to gambling, social selection, and probabilistic reasoning.

Materials and Methods

Experimental Setup

- Subjects perceive a specific direction upon viewing a random-dot stimulus. A mouse is used to move towards either a left or right target.
- The trial ends once the subject has reached one of the two targets.

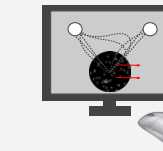


Figure 3. Experimental Setup. Schematic of the monitor viewed by the subject during the experimental session.

Timeline of Trial

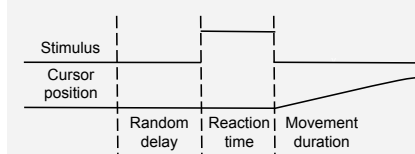


Figure 4. Timeline of Trial. The time course of events that make up a trial. Following a random delay, subjects viewed stimulus and indicated the direction of the dot motion by moving the cursor to leftward or rightward target. Motion stimulus vanished upon initiation of hand movement.

Coding

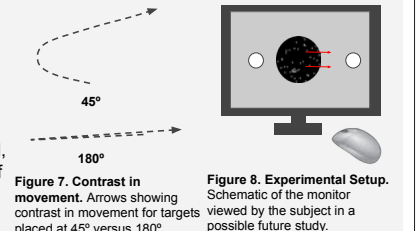
- Random dot stimulus is generated with Python, primarily tested with the PsychoPy IDE.
- The general structure of the experiment is based on the one presented in Resulaj's paper.
- Stimulus will be implemented on LiCoRICE machine to collect real-time data every millisecond of the cursor's position.



Figure 5. PsychoPy3 Logo. Primary IDE for development of the random dot stimulus used in experimental trials.

Future Directions

- We plan to expand on the study by placing targets at 180° and comparing this to data using 45° targets.
- We anticipate, since a less natural movement to change direction is required, the frequency of changes of mind will decrease.



References

- Pilly, P. K., & Seitz, A. R. (2009). What a difference a parameter makes: a psychophysical comparison of random dot motion algorithms. *Vision research*, 49(13), 1599–1612. doi:10.1016/j.visres.2009.03.019
- Resulaj, A., Kiani, R., Wolpert, D. M., & Shadlen, M. N. (2009). Changes of mind in decision-making. *Nature*, 461, 263-266.

Acknowledgements

This work was supported by the National Science Foundation through the UCLA Summer Undergraduate Research Program, specifically under the UCLA Electrical and Computer Engineering Department. We thank William Herrera and Muhammad Shahzain Raiz for their guidance throughout the program.



LAB NAME
Communications Systems Laboratory

FACULTY ADVISOR
Professor Richard Wesel


GRADUATE STUDENT DAILY LAB SUPERVISOR
Ethan Liang


DEPARTMENT
Electrical and Computer Engineering

Vincent Lau
Electrical Engineering
Third Year
UCLA



Design of Cyclic Redundancy Check (CRC) for Tail-Biting Convolutional Codes

Reliable transmission of data requires channel codes that can correct errors introduced by the channel and/or detect that a received or decoded sequence is not valid. Convolutional encoders can correct errors in a distorted received sequence by using the Viterbi algorithm to find the closest convolutional codeword to the received sequence. Cyclic redundancy check (CRC) codes can detect whether the convolutional codeword identified by Viterbi decoding corresponds to a valid message. While both CRCs and convolutional codes have been developed in the past, they have been designed independently even though they are not independent when used together. For zero-terminated convolutional codes (ZTCCs) that are terminated by a final sequence of inputs that drives the encoder to the zero state, our research group has designed CRCs that are optimal for a given ZTCC. Tail-biting convolutional codes (TBCCs) avoid the overhead caused by ZTCCs and therefore can achieve higher rates with essentially the same performance. Rather than using additional input symbols to drive the final state to zero, TBCCs enforce the constraint that the starting state is the same as the final state. Our research is directed towards developing CRCs that are optimal for a given TBCC.





Design of Cyclic Redundancy Check (CRC) for Tail-Biting Convolutional Codes
 Vincent Lau¹, Wenhui Sui¹, Ethan Liang¹, Richard Wesel¹
¹Communications Systems Laboratory, Department of Electrical and Computer Engineering
 University of California, Los Angeles

Introduction

Reliable transmission of data requires channel codes that can correct errors introduced by the channel and/or detect that a received or decoded sequence is not valid. Convolutional encoders can correct errors in a distorted received sequence by using the Viterbi algorithm to find the closest convolutional codeword to the received sequence. We are particularly interested in the implementation of tail-biting convolutional codes (TBCC), which reduce overhead and are capable of achieving higher rates at practically no expense to performance. Cyclic redundancy check (CRC) codes can detect whether the convolutional codeword identified by Viterbi decoding corresponds to a valid message. While both CRCs and convolutional codes have been developed in the past, they have been designed independently even though they are not independent when used together. Our research is directed towards developing CRCs that are optimal for a given TBCC. By first implementing an encoder and decoder for convolutional codes, we are building towards designing CRCs to ultimately accomplish this goal.




Figure 1. Overall system structure of convolutional code and CRC for communications.

Convolutional Codes

Convolutional codes are error-correcting codes that rely on memory storage in encoding, distinguishing them from traditional linear block codes. The encoder employs a shift-register structure that utilizes delay blocks to compute the output and track the state. We focus on rate-1/n encoders, which take 1-bit inputs and produce n-bit outputs.

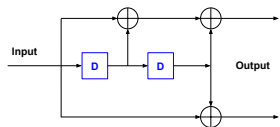


Figure 2. A convolutional encoder can be represented as a block diagram. The values inside the delay blocks (blue) represent the state of the encoder. [1]

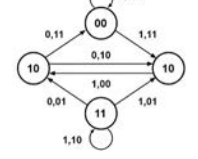


Figure 3. A state machine is used to determine the output for a particular input and state. It also shows the evolution of states in a compact way. [1]

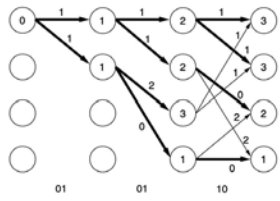
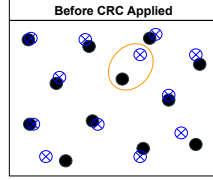


Figure 4. The Trellis diagram aids in keeping track of path metrics and surviving paths, which are utilized in Viterbi decoding. [1]

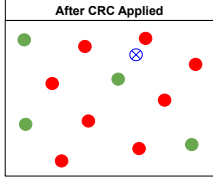
- The decoder we implement is based on the **Viterbi algorithm**, which can be realized with a Trellis diagram to keep track of the evolution of state paths over time, and helps us identify the most likely codeword given the received sequence.
- We are able to identify several performance metrics from the Trellis diagram, including free distance and number of nearest neighbors. The **free distance** represents the smallest Hamming distance between a pair of two valid codewords, while the number of nearest neighbors indicates the number of such pairs.
- While zero-terminated convolutional codes (ZTCCs) are terminated by a final sequence of inputs that drives the encoder to the zero state, **tail-biting convolutional codes (TBCCs)** require that the starting state be the same as the final state. These codes can achieve higher rates while maintaining nearly the same error-correcting performance.

Cyclic Redundancy Check (CRC)

Cyclic redundancy check (CRC) codes are error-detecting codes that help detect errors that may have been made by the decoder (e.g. the Viterbi decoder). At a high level, the CRC adds extra bits to the original codeword to serve as an extra layer of protection for decoding. This modification acts as an additional constraint to reduce the number of valid codewords, resulting in a smaller set of such valid codewords. This smaller set facilitates a larger minimum distance between codewords that provides a higher noise tolerance. In other words, the decoder will be less likely to select and validate an incorrect codeword.



Before CRC Applied



After CRC Applied

Figure 5. Visual representation of CRC operation: The figure at the left shows the space of valid codewords (black). Transmission over a channel creates noise, resulting in distortion in the received signals (blue). Sometimes the noise distorts the codewords so much that the decoder may associate the received signal with a different codeword (yellow), leading to an error in decoding. To limit this effect, the CRC will only pass specific codewords (green) and fail all others (red) to make the valid codewords distinct.

Materials and Methods

- This phase of the project primarily involved implementing a convolutional encoder and Viterbi decoder. This work was completed in MATLAB and was followed by extensive testing of both the codes and performance metrics for various examples of generator polynomials. We made sure to test different code rates and number of states.
- We started by simulating transmission across noiseless channels to make sure our encoder/decoder worked (i.e. zero errors occurred).
- For noisy channel transmission, we were interested in comparing bit-error rate (BER) vs. signal-to-noise ratio (Eb/No) for different rates and codes, as well as examining other properties like free distance, nearest neighbors, and analytic traceback depth.

Simulation Results

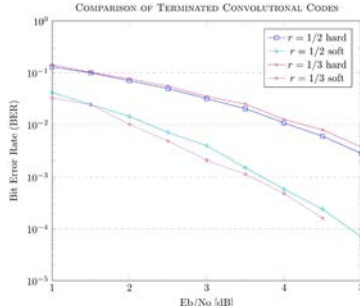


Figure 6. A performance comparison of bit-error rate (BER) vs. signal-to-noise ratio (Eb/No) between different generator polynomials for ZTCC. We tested codes with rate-1/2 and 1/3, which were decoded with both hard decision and soft decision.

- We compared two polynomials, (7,5) in purple and (13,12,16) in blue, which are of rate-1/2 rate-1/3, respectively.
- Two types of decoding were implemented and tested: hard-decision and soft-decision.
 - Hard-decision decoding uses a threshold value to decode a codeword.
 - Soft-decision decoding uses Euclidean distance to decode, which takes into account the impact of the noise on the transmission. Soft-decision decoding is the more refined and accurate technique of the two.
- As expected, the soft-decision decoding method outperformed the hard-decision decoding. Soft-decision required an Eb/No value about 2dB lower than hard-decision to produce the same BER.
- The rate-1/3 code performed better than the rate-1/2 code for soft-decision decoding, as expected. However, the two codes have similar performance for hard-decision decoding, which is an anomaly we are exploring (we expect the rate-1/3 to perform better).

Conclusions & Future Work

- Overall, our experience with the program was equal parts learning and re-implementing codes. We were able to develop a sound understanding of channel coding techniques and implement convolutional codes from scratch to supplement our learning process.
- For noiseless channels, we found that messages were decoded with zero error, as expected. Across noisy channels, noise was applied at different proportions, and we were also able to obtain good results (BER vs. Eb/No) for different parameters.
- We are looking towards the future to further develop our knowledge and bolster the significance of this project, with the ultimate goal of developing new CRCs for a range of CRC bit lengths. Specifically, we hope to eventually design new CRCs which are targeted for use with specific TBCCs, which we will implement.
- Our new CRCs will improve short-blocklength communications that are vital to sensor networks and the internet of things.

References

[1] R.D. Wesel, "Convolutional Codes", Wiley Encyclopedia of Telecommunications, John Wiley and Sons, 2003.
 [2] H.H. Ma, J.K. Wolf, "On Tail Biting Convolutional Codes", IEEE Transactions on Communications, 1986.
 [3] C.-Y. Lou, B. Daneshmand, R.D. Wesel, "Convolutional-Code-Specific CRC Code Design", IEEE Transactions on Communications, 2015.

Acknowledgments

We would like to thank the National Science Foundation and the Electrical and Computer Engineering Department for providing us the opportunity to conduct research. Additionally, we would like to acknowledge Ethan Liang and Hengjie Yang for providing guidance and mentorship throughout our research and learning process.



LAB NAME
Integrated Sensors Laboratory

FACULTY ADVISOR
Professor Aydin Babakhani

GRADUATE STUDENT DAILY LAB SUPERVISOR
Babak Jamali

DEPARTMENT
Electrical and Computer Engineering

Brandon Le
Electrical Engineering
Second Year
UCLA

Material Characterization Through THz-Wave Spectroscopy

Terahertz (THz) wave propagation allows for a large number of technological advances in modern systems, such as larger communication bandwidth and enhanced imaging resolution. THz wave signals also prove to be valuable in the practice of spectroscopy in order to characterize materials. The reason that THz waves present new advantages comes from two characteristics of millimeter waves. Because of their large bandwidth, these types of waves offer a larger absorption data set to uniquely identify materials. Secondly, their small wavelength nature allows these waves to have very high resolution in determining the thickness of a material.

This paper lays some groundwork of THz systems as a method of spectroscopy by testing its applications to solid materials. In our research, we set up a transmitter and a receiver to communicate with each other at varying sub-THz frequencies. An object of varying material is placed along the signal path to absorb some frequencies of communication dependent on the properties of that material. Intensity of the signals is measured at both the transmitter and the receiver and recorded in the frequency domain. Through a Support Vector Machine (SVM) machine learning algorithm, absorption plots obtained from various trials are used to identify the material obstructing the signal with 95% accuracy.



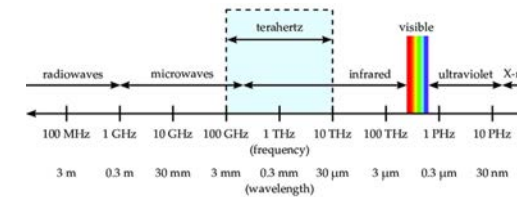
Material Characterization Through THz-Wave Spectroscopy

Brandon Le, Rachel Schwall, Babak Jamali, Aydin Babakhani



Background

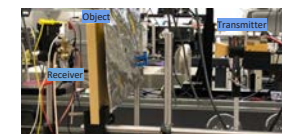
- Absorption spectroscopy is used to identify specific materials based on its absorption of various wavelengths of electromagnetic waves
- This practice is often used to determine if a particular substance is present and if so, how much
- Different methods exist for measuring absorption spectra but a common one is to analyze the intensity of the radiation that passes through the object



Introduction

- THz-waves pose a method of increasing the viable range of electromagnetic frequencies used for spectroscopy
- The goal of this experiment is to use a Support Vector Machine (SVM) algorithm to identify materials given its absorption of mm-waves
- SVMs classify data by determining an optimal hyperplane which acts as a separation boundary between different categories of data
- An SVM algorithm was used since it can effectively distinguish between complex sets of data, such as the various material absorptions, with much greater success than a human could

Materials and Methods



- Signal power received by the circuit was measured in the presence and absence of an object



- Absorption for each object was calculated by taking the difference in power with and without the object

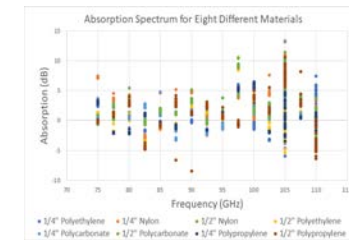


- The SVM algorithm drew decision boundaries to differentiate the different materials' absorption data

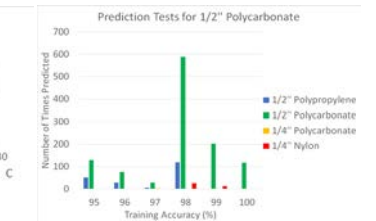
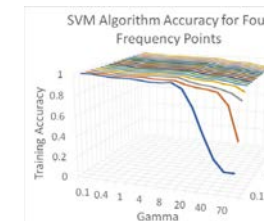
References

Jamali, Babak and Babakhani, Aydin. "A Fully Integrated 50–280-GHz Frequency Comb Detector for Coherent Broadband Sensing".
Pätzold, Martin. "Graphical Models and Simulation for THz-Imaging," *PhD Dissertation*, (2018).

Results



- An example of absorption data supplied to the SVM algorithm
- The SVM algorithm allows the machine to understand small differences in absorption that we could not observe ourselves for classification
- For these tests, absorption data at 105 and 110 GHz for all materials were unreliable, and thus were not necessarily used for training



- The SVM algorithm was most accurate when using between two and six frequency points for training and using a low value for gamma
- For this range, the value of C didn't affect the accuracy very much
- This graph shows the frequency of predicting different materials from a new set of absorption data separate from the training
- For 95% training accuracy and above, an SVM algorithm proves effective in classifying the correct material over other possibilities

Conclusion/Future Works

Conclusion:

- From absorption spectra measurements, a Support Vector Machine algorithm can be trained to predict the material obstructing the signal with 95% accuracy
- Given new test data after training, higher training accuracy is required for consistently accurate classifications of objects

Future Works:

- Using other machine learning algorithms to separate absorption data and determine if other algorithms prove more accurate in predicting materials
- Create new absorption data to determine if other factors besides material type and thickness affect absorption
- Running these tests with a new set of materials to provide more data and materials for machine learning algorithms to classify

Acknowledgements

We would like to thank the UCLA Summer Undergraduate Research Program for this research opportunity and the ECE Dean's Department for funding the experience. We would also like to thank Professor Babakhani for providing the opportunity to work in his lab as well as Babak Jamali for his support and guidance throughout the program.



Michael Molter
Electrical Engineering
Third Year
UCLA

LAB NAME
Center for Heterogenous Integration and Performance Scaling (CHIPS)

FACULTY ADVISOR
Professor Subramanian Iyer

GRADUATE STUDENT DAILY LAB SUPERVISOR
Arsalan Alam

DEPARTMENT
Electrical and Computer Engineering

Design of Flexible, Wireless Surface Electromyography System

According to the CDC 1 in every 7,250 males are afflicted by Duchenne and Becker muscular dystrophy, a disease that affects muscle strength and leads to muscle degeneration. Surface Electromyography (EMG) is a non-invasive method used to measure muscle activity that can help in the diagnosis and treatment of musculoskeletal diseases such as muscular dystrophy. Typical Surface Electromyography machines are often bulky, rigid, and heavy which makes them difficult to use in a clinical setting, and it means they cannot be used as wearable devices. In addition, these systems are often single-channel systems which limit the spatial and temporal information that the system can gather, making readings incomplete. To help solve these issues, a full multi-channel electromyography system that is lightweight, flexible, and wireless will be integrated on FlexTrate™, a flexible electronic platform based on Fan-Out Wafer Level Packaging (FOWLP). The surface EMG will take advantage of FlexTrate™ to integrate a variety of different integrated circuit (IC) dies such as amplifiers, passive components, and a Bluetooth Low Energy (BLE) chip as well as electrodes to detect the EMG signal. For wireless communication, the Nordic nRF52840 BLE module is used for low system power. Using FlexTrate™, the overall system will be lightweight, thickness less than 1 mm, and flexible enough to conform to skin allowing for a wearable device that can be used easily in a clinical setting.

Fast Track to SUCCESS
summer scholars program
Electrical Engineering Department
@UCLA

Functional Nanomaterials
UCLA ENGINEERING
Summer Scholars Program

Design of Flexible, Wireless Surface Electromyography System

M. Molter, A. Alam, and S. S. Iyer (UCLA CHIPS)

UCLA Samueli
School of Engineering
Summer Undergraduate Research Program

Motivation

- According to the CDC Muscular dystrophy effects 1 in 7250 males
- Surface Electromyography (EMG) measures the electrical activity of muscles for diagnoses of muscular disorders
- Existing Surface Electromyography systems are bulky, non-flexible, and heavy making them difficult to use
- FlexTrate™ is a flexible electronic platform based on Fan Out Wafer Level Packaging allowing integration of high performance dies
- FlexTrate™ is an ideal platform for a complete flexible and lightweight EMG system due to flexibility and ability to integrate many high performance dies

Traditional Surface Electromyography

System Design

Surface EMG on FlexTrate™ Layout

In the figure below, we see the simple layout and size of EMG system. Total system thickness will be less than 1 mm and weigh approximately 10 g.

FlexTrate™ Surface EMG Electrodes Bent and Rolled

Verification of Wireless Communication Cont.

A comparison of EMG signals gathered simultaneously from an oscilloscope and Bluetooth controller. We can see that the EMG signals are visually the same from both.

Control Electronics

The control electronics amplify the EMG signal from microvolts to a voltage readable by the Bluetooth ADC.

The Nordic 52840 BLE chip sends data wirelessly to central computer

Signal Post Processing

Filtering Process

Surface EMG signals have only been recorded in the range of 5 – 500 Hz allowing filtering outside those ranges. Filtering allows removals of DC and low frequency noises associated with wire movement below 5 Hz and high frequency noises above 300 Hz.

The pre and post processed signals Filtered EMG signal can be seen in the figure to the right.

In the close up view, we can see the pre-processed signal is subject to a large power line noise. Removing noise allows us to clearly see muscle activation signals that are not visible before.

Verification of Wireless Communication

Cross Correlation of a sinusoid from a signal generator was recorded simultaneously from an oscilloscope and our Bluetooth controller at 10 Hz and 500 Hz. High correlation coefficients of 0.9923 and 0.9545 were calculated from cross correlation of both signals sources.

Conclusions/Future and Ongoing Work

Demonstrated the beginning steps towards a fully flexible, wireless, and lightweight surface EMG system including:

- Flexible electrodes
- Robust Wireless system capable of recording EMG
- Design of control electronics

Full System integration onto FlexTrate™ including the Bluetooth controller and control electronics.

References/Acknowledgements

[1] M.B.I Raez et al. Techniques of EMG signal analysis: detection, processing, classification and applications, Biol Proced, 2006
 [2] G. Ezhilarasu et al., IEDM, 2019.
 [3] Romitti PA, Zhu Y, Puzhankara S, et al. Prevalence of Duchenne and Becker Muscular Dystrophies in the United States, Pediatrics. 2015

I would like to acknowledge CHIPS at UCLA for allowing me to research this summer as well as the UCLA engineering and SURP for providing their support for undergraduate research.



LAB NAME
UCLA Plasma Accelerator Group

FACULTY ADVISOR
Professor Chandrashekhar Joshi

GRADUATE STUDENT DAILY LAB SUPERVISOR
Zan Nie

DEPARTMENT
Electrical and Computer Engineering

Noa Nambu
 Electrical Engineering
 Third Year
 UCLA

Spin-polarized Electrons by Photoionization with Intense Ultrashort Lasers

High-energy spin-polarized electrons are important for the investigation of pathways in high-energy collisions. However, generation of such electrons is difficult using conventional methods. Photoionization is a very common phenomenon that shows potential to provide a simpler way to produce spin-polarized electrons. Developments in laser technology have made it possible to create extremely high intensity light, which leads to various ionization processes. Multiphoton ionization involves the transfer of energy from multiple photons to an electron in order to surpass the ionization potential. Tunneling ionization occurs when higher field strength and lower frequencies allow the laser to be treated as an electric field which changes the shape of the potential barrier and allows the electron to escape through tunneling. The rates of ionization in these regimes have been described by several theories developed by Landau, Keldysh, ADK, PPT, and Barth and Smirnova. Different models of ionization rates were compared in order to find the areas in which they can be used to accurately describe ionization. The incorporation of magnetic and angular momentum quantum numbers into ionization rates allows for selective ionization of spin-polarized electrons, leading to predictions of up to 30% spin polarization. This may open a new avenue for the generation of high-energy, spin-polarized electrons in combination with the laser wakefield acceleration technique.

UCLA Samueli School of Engineering
 Summer Undergraduate Research Program

Spin-polarized Electrons by Photoionization with Intense Ultrashort Lasers

Noa Nambu, Zan Nie, Ken Marsh, Chan Joshi
 Department of Electrical and Computer Engineering
 University of California, Los Angeles

NSF

Introduction

- High-energy spin-polarized electrons are of interest to high-energy and particle physics, which are very difficult to generate by conventional methods.
- Laser technology has made it possible to create extremely high intensity light, suitable for tunneling and multiphoton ionization. Theories by Landau, Keldysh, ADK, PPT, and Barth and Smirnova describe rates of photoionization.
- Photoionization shows potential to provide a simpler way to produce spin-polarized electrons

Multiphoton and Tunneling Ionization

- Keldysh parameter differentiates multiphoton or tunneling
- $\gamma = \frac{\omega(2mI_p)^{1/2}}{E}$
- Multiphoton ionization ($\gamma > 1$) occurs when the energy of a single photon is lower than the ionization potential, but the intensity is high enough that multiple photons can interact with the electron at once
- Tunneling ($\gamma < 1$) occurs at higher intensities and lower frequency, where the electric field changes the shape of the potential barrier and allows the electron to escape by tunneling

Barrier Suppression Ionization

- High enough electric fields will deform the potential barrier to the point that an electron can freely escape without tunneling
- Critical field: $E_c = \frac{I_p^2 \epsilon_0}{2e^2}$

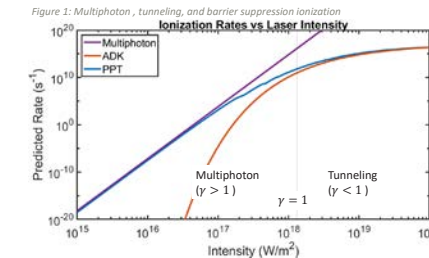
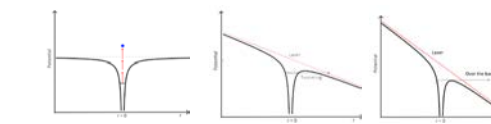


Figure 2: Ionization rates of Ar in 800 nm light predicted by different models: ADK (tunneling), multiphoton, and PPT.

Temporal Evolution of Ionization by Laser Pulse

- Electric field can be expressed as either a carrier or envelope, but using corrected rates yields similar results for ionization
- $E = E_0 \exp\left(\frac{t^2}{2\sigma^2}\right) \cos(\omega t)$ $I = \frac{|E_0|^2}{2\epsilon_0}$

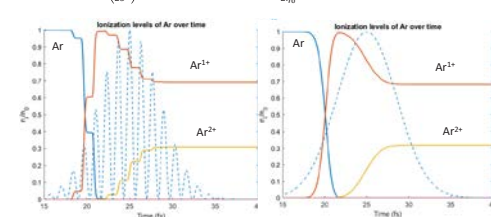


Figure 3: Ionization of Ar over time by laser pulse. Pulse is 12 fs with 800 nm light, 10^{14} W/cm^2 peak intensity. Instantaneous (left) vs time-averaged (right)

References

M. V. Ammosov, N. B. Delone, and V. P. Krainov, *Sov. Phys. JETP* **64**, 1191 (1986).
 Augst, S., Meyerhofer, D.D., Strickland, D. & Chin, S.L. (1991). Laser ionization of noble gases by Coulomb-barrier suppression. *J. Opt. Soc. Am. B*, **8**, 858-867.
 L. V. Keldysh, "Ionization in field of a strong electromagnetic wave," *Sov. Phys. JETP* **20**, 1307-1314 (1965).
 A. M. Perelomov, V. S. Popov, and M. V. Terentev, "Ionization of atoms in an alternating electric field," *Sov. Phys. JETP* **50**, 1393-1409 (1966).
 Jens Schwarz, Patrick Rambo, Mark Kimmel, and Briggs Atherton, "Measurement of nonlinear refractive index and ionization rates in air using a wavefront sensor," *Opt. Express* **20**, 8791-8803 (2012).
 I. Barth and O. Smirnova, *Phys. Rev. A* **84**, 063415 (2011)

Electron orbitals

- Bound electrons have quantized energy levels, angular momentum, and projection of angular momentum, given by n , l , and m quantum numbers
- m quantum number describes the projection of the angular momentum onto an axis

m-dependent Ionization Rates

- For p-electrons exposed to circularly polarized light, projection of angular momentum onto the direction of the light can be seen as a sense of rotation of the electron
- Counter-rotating electrons have a higher ionization rate, than co-rotating electrons
- For linearly polarized light, $m = 0$ has the highest ionization rate

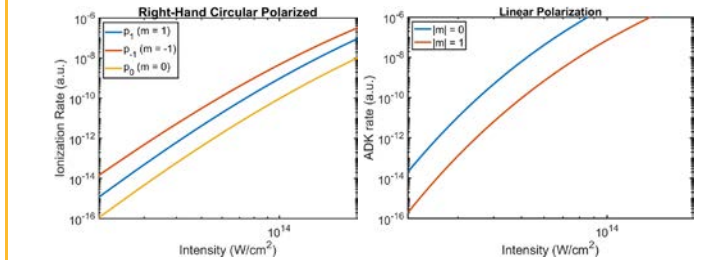


Figure 3: Different ionization rates for p-electrons of Ar depending on their magnetic quantum number in both linearly (right) and circularly (left) polarized light, using Barth and Smirnova's extension to PPT and the ADK model.

Summary of Models

Model	Range of γ	Atomic shell	Polarization	AC or DC
BSI	High intensity field above critical field	Doesn't depend on shell	Doesn't depend on polarization	Instantaneous
Landau	DC Tunneling ($\gamma < 1$)	Hydrogen ($n=1, l=m=0$)	N/A	DC
Keldysh	Multiphoton and tunneling	Hydrogen ($n=1, l=m=0$)	Linear	Time-averaged
ADK	Tunneling ($\gamma < 1$)	Any n, l, m	Linear, circular for s-orbitals	Instantaneous, time-averaged for linearly polarized
PPT	Multiphoton and tunneling	Any n, l, m	Linear, circular for s-orbitals	Time-averaged?
Barth and Smirnova	Multiphoton and tunneling	Any n, l, m	p-orbitals with circularly polarized light	Time-averaged?

Spin Selectivity

- Spin is coupled to m numbers, so selecting for m allows spin-selectivity
- ionization into the $^2P_{3/2}$ state has a lower ionization potential, and occurs at a higher rate

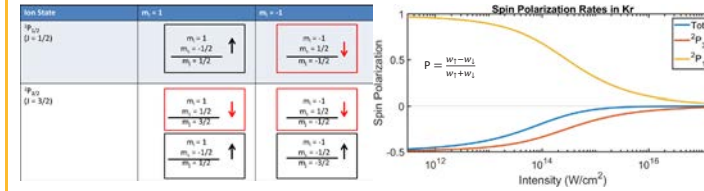


Figure 4: Spin polarization based on ionization rates in Kr

Conclusions and Future Work

- Different theories of ionization are investigated and summarized to gain an understanding of photoionization under many conditions
- Theories of multiphoton and tunneling ionization predict that spin-polarized electrons can be generated by photoionization This can be combined with the laser wakefield acceleration technique to create high-energy spin-polarized electrons



LAB NAME
Speech Processing and Auditory Perception Laboratory

FACULTY ADVISOR
Professor Abeer Alwan


GRADUATE STUDENT DAILY LAB SUPERVISOR
Gary Yeung

DEPARTMENT
Electrical and Computer Engineering

Robert Ozturk
 Electrical Engineering
 First Year
 UCLA

Automated Speech Database Organization



The development of an autonomous social robot, able to deliver clinical and educational assessments to young children, has great potential to aid in the efforts of educators and help students reach age-appropriate levels of proficiency in reading and oral language skills. A study researching the feasibility of the JIBO robot for such purposes, as well as gathering data needed to improve child automated speech recognition (ASR), resulted in a large dataset of verbal interactions between the robot and children via the administration of the Goldman-Fristoe Test of Articulation (GFTA) and other language tasks. Prior to database publication, time consuming and error-prone tasks such as matching audio data with corresponding prompt-answer pairs and the notation of private information for removal must be performed. We present a design and Python implementation for software automating and simplifying such processes. As robot prompts are known and consistent, timestamps are detected in audio files using a cross-correlation approach. We propose several methods of avoiding computationally expensive operations during such a search. For files with transcripts, processing is done using both a brute force search and the SpaCy natural language processing package, the latter to identify possible private information. Results are compared and combined with those from audio processing. Finally, we propose a database organizational structure and documentation in preparation for future publication.



UCLA Samueli
 School of Engineering
 Summer Undergraduate
 Research Program

Automated Speech Database Organization
 Robert C. Ozturk¹, Dan Song¹, Gary Yeung¹ and Abeer Alwan¹

¹Department of Electrical and Computer Engineering,
 University of California, Los Angeles

Introduction




Figure 1. The JIBO personal assistant robot was released in November of 2017.

- What if a robot could help in the classroom?
- Recent research by Yeung et al. (2019) explored the feasibility of having the social robot JIBO (Figure 1) deliver educational assessments to young children [1].
- Additionally, data it produced was intended to be used towards developing better child automatic speech recognition (ASR), the current state of which has held back child human-robot interaction research [2].
- JIBO's administration of a letter and digit naming task and the 3rd Goldman Fristoe Tests of Articulation (GFTA-3) resulted in a large database containing 60 hours of child-robot interaction.
- This work presents an attempt to automate the necessary pre-processing of this database, as well as propose a database organizational structure.

Design: Audio Processing

- Template-based recognition was used to perform time-delay estimation to find robot speech in an audio file (Figure 2). Results shown in Figure 3.

Figure 2. Flow-chart of template-based recognition

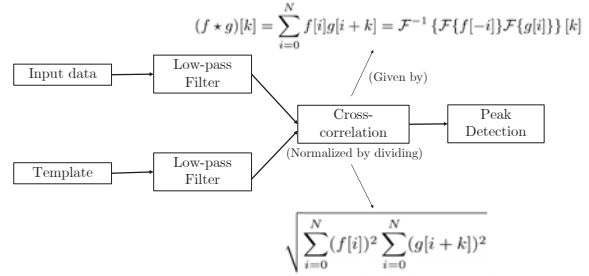
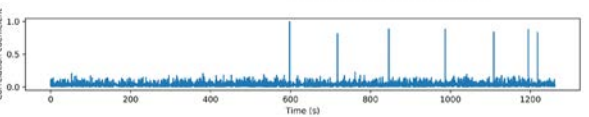
$$(f * g)[k] = \sum_{i=0}^N f[i]g[i+k] = \mathcal{F}^{-1} \{ \mathcal{F}\{f[-i]\} \mathcal{F}\{g[i]\} \} [k]$$



Figure 3. Results of one normalized cross-correlation. The large peaks are matches to some JIBO voice line. A vertical axis value of 1 indicates an exact match. Due to noise and microphone placement inconsistencies, an exact match was very rare and thresholding was used to determine whether a match took place.

Database

Subjects and Recordings:

- 156 children were recorded interacting with JIBO over 236 sessions.
- Sessions lasted between 5 and 40 minutes.
 - Session length varied based on child engagement and experience.
- Children were recorded in a classroom study space with limited noise.

Tasks:

- 3rd Goldman Fristoe Tests of Articulation (GFTA-3)
- Letter and digit naming task

Transcriptions:

- Full transcripts of the audio were produced by trained transcribers.
- Phonetic transcriptions were produced by trained phoneticians.

Deliverables

- A new database layout was designed and accompanied with documentation using combined data from the designed processing methods.
- User interface was created for labeling and cutting audio. It decreases manual work by giving the user certain features:
 - Jump to audio containing private info or the beginning of certain tasks
 - Switch between textual and audio analysis (Figure 4) of child interviews

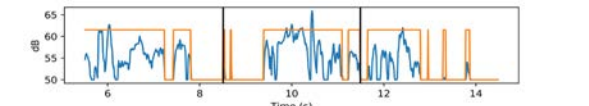





Figure 4. A small section of a sound file. The user selected section is between the two black vertical lines. The orange sound blocks can be snapped to while scrubbing or can be ignored if fine scrubbing is desired.

Methods

/^ [Regular] [Expression] \$ /

Design: Text Processing

- Processing of audio transcripts was utilized in multiple ways:
 - To extract task completion data for documentation
 - To identify private information
 - As a guiding tool when labeling and cutting audio
- Regular expression (regex) use on the predictable transcript layout allowed for such analysis.
 - Ex. “\((\d+:\d\d)\)” searches for timestamps of the form (min:sec)
- spaCy:
 - This open-source package for Natural Language Processing aided in identifying private information within files, decreasing manual work.
 - Part-of-Speech tagging and Named Entity Recognition (NER) were the two main features of the package utilized.

Conclusion and Future Work

- This database will assist in research for a number of diverse applications:
 - Child automatic speech recognition
 - Child speech science and linguistics
 - Human-robot interaction
- Going forward, we hope to generalize the methods for preliminary processing to all speech databases.

References

[1] Yeung, G., Afshan, A., Quintero, M., Martin, A., Spaulding, S., Park, H. W., ... and Alwan, A. (2019). Towards the development of personalized learning companion robots for early speech and language assessment. *2019 Annual Meeting of the American Educational Research Association (AERA)*.

[2] Yeung, G., & Alwan, A. (2018). On the Difficulties of Automatic Speech Recognition for Kindergarten-Aged Children. *Interspeech*, 1661–1665.

We would like to thank Professor Alwan, Gary Yeung, Amber Afshan, and Morgan Tinkler for the opportunity, guidance, and warm welcome given to us. Additional thanks to the UCLA Wireless Health Institute, UCLA ECE Fast Track Program, and the NSF for their continuing support, financially and otherwise, for undergraduate research.



LAB NAME
Algorithmic Research in Network Information Flow Laboratory

FACULTY ADVISOR
Professor Christina Fragouli

GRADUATE STUDENT DAILY LAB SUPERVISOR
Yahya Ezzeldin

DEPARTMENT
Electrical and Computer Engineering

Tara Sadjadpour
 Electrical Engineering
 Third Year
 UCLA

Distributed Quantization for Classification Tasks

When using quantization schemes for distributed classification, the goal is not to reconstruct quantized data perfectly; rather, it is to create a quantization approach such that the classifier maintains the accuracy it had before the large, high-precision data was quantized. If a communication quality constraint exists between different devices in the system, then the number of bits that can be used in our quantization approach is further limited. In applications, such as brain-machine interface and Google Cloud Internet of Things, there is a pretrained classifier that resides in a central node in a communication network, where it receives unclassified data that is distributedly generated. In the case of brain-machine interface, sensors are distributed on a subject's body, and thus, high-precision features are generated from these body parts. This data is then classified for an actuator to carry out some action. Previously published solutions present a greedy algorithm that uses a recursive binning technique to quantize the data. We propose a more efficient, adaptable quantization approach implemented with neural networks. This approach achieves approximately the same accuracy as the greedy algorithm on an sEMG dataset with lower time complexity.



UCLA Samueli School of Engineering
 Summer Undergraduate Research Program



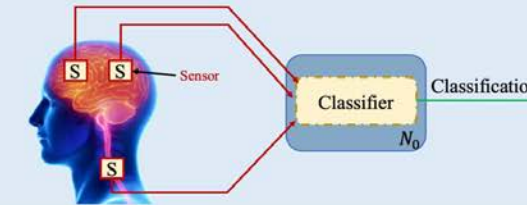
Distributed Quantization for Classification Tasks

Tara Sadjadpour, Yahya Ezzeldin, Christina Fragouli

Algorithmic Research in Network Information Flow Laboratory, Dept. of Electrical and Computer Engineering

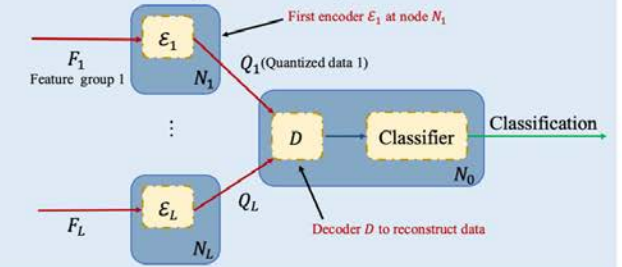
Distributed Classification

- **Applications:** Brain-Machine Interface, Google Cloud Internet of Things
- **Model:** A pretrained classifier resides in a central node, N_0 , in the communication network, where it receives data features that are generated at distributed nodes, e.g. in brain-machine interface.

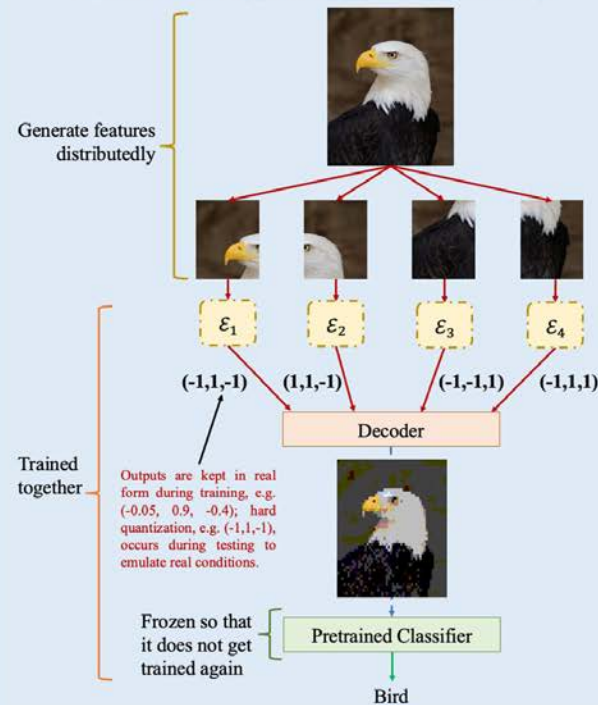


Motivation and Problem Statement

- **Challenge:** Transmitting features at original size requires too many resources for large, high-precision data points.
- **Enforcing Communication Constraints:** Use encoders located at distributed nodes to send fewer bits in place of the original data.
- **Goal:** The aim is not to perfectly reconstruct quantized data, but to create a quantization approach (i.e., encoder-decoder) such that the classifier maintains the accuracy it had with the original data.



Quantization Approach with Deep Learning



Future Directions

- Improve the accuracy of the quantization approach with different data sets.
- Analyze loss function for theoretical guarantees.

References

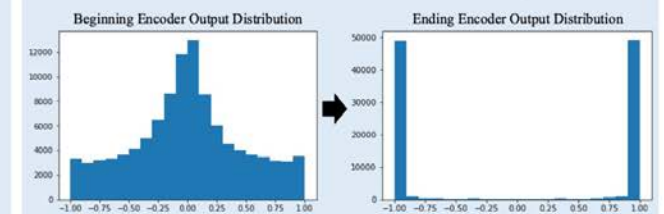
- [1] O. Hanna et al. "Distributed Quantization for Classification" (2019).
 [2] S. Lobov, N. Krilova, I. Kastalskiy, V. Kazantsev, and V. Makarov, "Latent factors limiting the performance of sEMG-interfaces," (Sensors 2018).

Performance of Our Quantization Approach

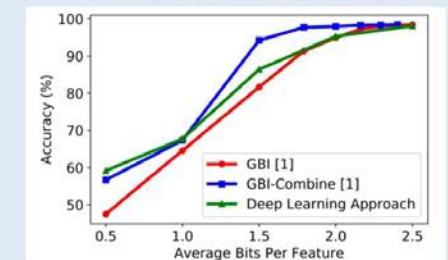
- **Loss Function:** Our goal is to minimize the following loss:

$$\mathcal{L} = - \sum_{i=1}^N \hat{y}_i + \log \left(\sum_{i=1}^N \exp(\hat{y}_i) \right) + \frac{1}{L} \sum_{l=1}^L \sum_{j=1}^M (1 - \varepsilon_{ij}^2)$$

Trains for correct classification Trains encoder outputs toward ± 1



- **sEMG Data Set [2]:** 8 sensors were placed on subjects' forearms to detect 6 possible hand gestures. We compare our quantizer's classification accuracy with that of previously published quantizers for this dataset [1].



- **Trade-off:** Though the accuracy for our deep learning approach is not as high as GBI-Combine's, our new quantizer has significantly higher efficiency than GBI and GBI-Combine.



LAB NAME
Integrated Sensors Laboratory

FACULTY ADVISOR
Professor Aydin Babakhani

GRADUATE STUDENT DAILY LAB SUPERVISOR
Babak Jamali

DEPARTMENT
Electrical and Computer Engineering

Rachel Schwall
Electrical Engineering
Second Year
UCLA

Absorption Spectroscopy Using Millimeter-Wave and Sub-Terahertz Frequencies

Sensing and retrieving data from millimeter-wave and sub-terahertz frequencies are useful for many different applications including faster data transmission in wireless communication and enhanced resolution in imaging systems. In this frequency regime, broadband systems are also useful for spectroscopy and detecting different absorption frequencies of gas molecules. A comb-based method can be used to enhance bandwidth to include these frequencies and coherent detection techniques can be used to implement a receiver that can detect them. Integrated circuits designed using this method exhibit improved bandwidth, and detection resolution as well as reduced power consumption compared to current CMOS wideband coherent receivers. One specific use for these transmitter and receiver circuits is absorption spectroscopy where the power of the signal generated by the transmitter is measured after it passes through a specific material and is recorded by the receiver. A support vector machine (SVM) algorithm can then be trained with the absorption data of multiple materials to identify a new material given its absorption data collected from the receiver. SVMs are machine learning models that can classify data by determining an optimal hyperplane which acts as a separation boundary between different categories of data. An algorithm that utilizes SVM is quite effective when it comes to distinguishing between complex sets of data since it is able to determine boundaries in the data that may not be the most obvious to the human eye.



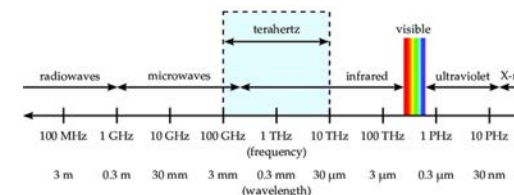
Material Characterization Through THz-Wave Spectroscopy

Rachel Schwall, Brandon Le, Babak Jamali, Aydin Babakhani



Background

- Absorption spectroscopy is used to identify specific materials based on its absorption of various wavelengths of electromagnetic waves
- This practice is often used to determine if a particular substance is present and if so, how much
- Different methods exist for measuring absorption spectra but a common one is to analyze the intensity of the radiation that passes through the object



Introduction

- THz-waves pose a method of increasing the viable range of electromagnetic frequencies used for spectroscopy
- The goal of this experiment is to use a Support Vector Machine (SVM) algorithm to identify materials given its absorption of mm-waves
- SVMs classify data by determining an optimal hyperplane which acts as a separation boundary between different categories of data
- An SVM algorithm was used since it can effectively distinguish between complex sets of data, such as the various material absorptions, with much greater success than a human could

Materials and Methods



- Signal power received by the circuit was measured in the presence and absence of an object



- Absorption for each object was calculated by taking the difference in power with and without the object

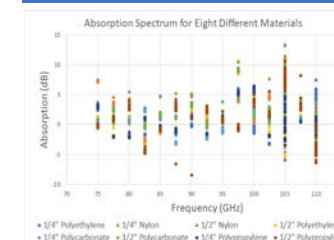


- The SVM algorithm drew decision boundaries to differentiate the different materials' absorption data

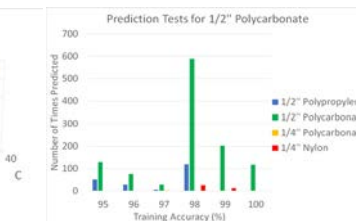
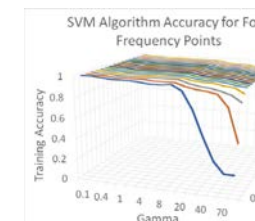
References

Jamali, Babak and Babakhani, Aydin. "A Fully Integrated 50–280-GHz Frequency Comb Detector for Coherent Broadband Sensing".
Pätzold, Martin. "Graphical Models and Simulation for THz-Imaging," *PhD Dissertation*, (2018).

Results



- An example of absorption data supplied to the SVM algorithm
- The SVM algorithm allows the machine to understand small differences in absorption that we could not observe ourselves for classification
- For these tests, absorption data at 105 and 110 GHz for all materials were unreliable, and thus were not necessarily used for training



- The SVM algorithm was most accurate when using between two and six frequency points for training and using a low value for gamma
- For this range, the value of C didn't affect the accuracy very much
- This graph shows the frequency of predicting different materials from a new set of absorption data separate from the training
- For 95% training accuracy and above, an SVM algorithm proves effective in classifying the correct material over other possibilities

Conclusion/Future Works

Conclusion:

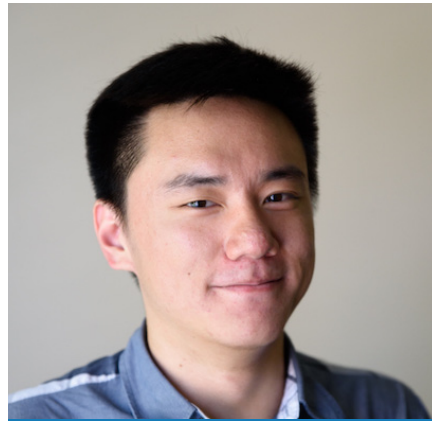
- From absorption spectra measurements, a Support Vector Machine algorithm can be trained to predict the material obstructing the signal with 95% accuracy
- Given new test data after training, higher training accuracy is required for consistently accurate classifications of objects

Future Works:

- Using other machine learning algorithms to separate absorption data and determine if other algorithms prove more accurate in predicting materials
- Create new absorption data to determine if other factors besides material type and thickness affect absorption
- Running these tests with a new set of materials to provide more data and materials for machine learning algorithms to classify

Acknowledgements

We would like to thank the UCLA Summer Undergraduate Research Program for this research opportunity and the ECE Dean's Department for funding the experience. We would also like to thank Professor Babakhani for providing the opportunity to work in his lab as well as Babak Jamali for his support and guidance throughout the program.



LAB NAME
Sensors and Technology Laboratory

FACULTY ADVISOR
Professor Rob Candler

GRADUATE STUDENT DAILY LAB SUPERVISOR
Jimmy Wu

DEPARTMENT
Electrical and Computer Engineering

Justin Shao
Electrical Engineering
Second Year
UCLA

Millimeter-Scale Electroplated Multilayer Magnetic Shielding

Many devices that rely on atomic spectroscopy, like gyroscopic sensors and atomic clocks, require magnetic shielding to function as intended because of interference by external magnetic fields. Although no known material is able to stop a magnetic field, high permeability materials are able to effectively redirect magnetic field lines, creating protected regions of low magnetic field strength. Current methods of magnetic shielding involve inserting a sheet of high permeability material on a circuit board underneath a device or wrapping a region in a sheet of the high permeability material. In this project, we fabricate high performance chip-scale magnetic shields by electroplating alternating layers of nickel-iron alloy, which has a high relative permeability, and copper, which has a low relative permeability, onto a cylindrical shell. By alternating layers of high and low permeabilities, we minimize the influence of the demagnetization field, achieving a higher ability to redirect magnetic field lines. To test the shields, we use an electromagnet to generate a magnetic field and a magnetometer to measure the magnetic field inside the shield. We record the shielding factor of the shield, which is defined as the ratio of the external magnetic field strength to the internal magnetic field strength. Successful millimeter-scale shielding would allow for effective chip-scale implementation of devices that would function in external magnetic fields while conserving space.

Millimeter-Scale Electroplated Multilayer Magnetic Shielding

UCLA Samueli School of Engineering
Summer Undergraduate Research Program

Justin Shao, Sydney Walsh, Hou Seng Wong, Jimmy C. Wu, and Rob N. Candler*
Sensors and Technology Laboratory, Electrical and Computer Engineering Department, University of California, Los Angeles*



Introduction

Motivation

- Devices like atomic clocks and sensors require magnetic shielding because of sensitivity to external magnetic fields
- Using high magnetic permeability materials, magnetic shields can create protected regions of low magnetic field
- Current machining methods are limited to larger scales
- We use electroplating to fabricate more compact and efficient magnetic shields
- Successful implementation of chip-scale magnetic shields can lead to new innovations like GPS-free location tracking

Jackson, 1998
Illustration of shielding effect

Design and Fabrication

Magnetic Shielding Mechanism

External magnetic field

Magnetization in a material follows a nonlinear curve and maximizes at saturation

External field magnetizes material

Magnetization of a region opposes magnetization of neighboring regions

Fields from magnetization and external magnetic field cancel out near the material

Multilayer Shielding Design

Magnetic field of red region opposes magnetization of blue regions

- Magnetization of a region opposes magnetization of neighboring regions
- By removing a layer of magnetic material, the neighboring regions reach higher magnetization
- A multilayer shield can better oppose external magnetic fields

Fabrication

Sulfate solution
copper sulfate for plating copper layers; iron sulfate and nickel sulfate for depositing permeable layers

The positively charged ions are attracted to the cathode.

The negatively charged sulfate ions are attracted to the anode.

The ions deposit the metal on the cathode.

We use electroplating to deposit thin, even layers onto a cylindrical wax mold

After electroplating, the wax mold is dissolved in xylene, leaving just the metal shell

Results

Measurement Procedure

Shielding factor measurement setup

Power Supply & Waveform Generator, Hall Effect Probe, Shield Under Test, Electromagnet, Gaussmeter, Probe Mount, Mumetal Shield Layers

Wu, J. et al., 2017

Flexible Magnetic Sensor PCB

Magnetic Sensor, Electronics, Printed circuit board with magnetometer for measuring magnetic field

- We apply a known magnetic field to a magnetometer using an electromagnet
- Measure the magnetic field using a magnetometer inside the magnetic shield
- Calculated shielding factor defined as $S \equiv \frac{H_{external}}{H_{internal}}$

Experimental Results

Shielding Factor vs. External Magnetic Flux Density

Shielding Factor

External Magnetic Flux Density (G)

Internal magnetic flux density and shielding factor plotted against external magnetic flux density

Internal vs. External Magnetic Flux Density

Shielded Magnetic Flux Density (G)

Unshielded Magnetic Flux Density (G)

Internal magnetic field plotted against external magnetic field

From our experiments, the shield is most effective at in weaker magnetic fields. The performance of the shield decreases as the magnetic field gets stronger because the magnetic material in the shield approaches saturation, and its ability to cancel magnetic fields reaches a maximum.

COMSOL Physics Simulation

Cross sectional views of a simulated cylindrical shield inside a uniform external magnetic field

Simulation of magnetic flux density in a multilayer cylindrical shield

We demonstrate the magnetic shielding effect in COMSOL Multiphysics simulations, showing that the magnetic field is concentrated within the shield's material and redirected around the region enclosed by the cylinder.

Discussion and Future Work

Results Analysis

In comparison with current methods of magnetic shielding, our cylindrical shield is more effective at protecting regions from magnetic fields. For weaker magnetic fields, we recorded shielding factors higher than 400, while a flat sheet of similarly high permeability metal, as those found in current methods of magnetic shielding, could not achieve a shielding factor higher than 1.2.

Future Work

- Shielding factor greatly dependent on geometry of the shield
- From Maxwell's equations, the magnetic field around the surfaces of the magnetic material satisfies the boundary conditions at every surface:

$$(B_2 - B_1) \cdot \hat{n} = 0$$

$$(H_2 - H_1) \times \hat{n} = 0$$
- Using electroplating to generate the shields, it is possible to create shields of more complex geometries not achievable with traditional machining methods

x, y, and z components of internal magnetic fields within the protected regions of the plate and cylinder shaped shields

Acknowledgements

We would like to acknowledge the UCLA Summer Undergraduate Research Program, the UCLA Electrical and Computer Engineering Department, National Science Foundation, Functional Nanomaterials, the Sensors and Technology Laboratory. We would also like to acknowledge Erik Hodges, the previous undergraduate who worked on this project.

References

Jackson, John David (10 August 1998). *Classical Electrodynamics* (third ed.). "NIST Unveils Chip-Scale Atomic Clock." NIST, 21 Mar. 2018. www.nist.gov/news-events/news/2004/08/nist-unveils-chip-scale-atomic-clock.

Wu, J., Li, L., Harrison, J., and Candler, R. Micro- to Millimeter Scale Magnetic Shielding, 2017.

NIST, 2018
Chip-scale atomic clock

59



LAB NAME
Laboratory for Embedded Machines and Ubiquitous Robots (LEMUR)

FACULTY ADVISOR
Professor Ankur Mehta

GRADUATE STUDENT DAILY LAB SUPERVISOR
Professor Ankur Mehta

DEPARTMENT
Electrical and Computer Engineering

Shantinath Smyth
 Electrical Engineering
 Second Year
 UCLA

Custom Printable Robotic Boats for Early STEM Education

Robotics engages students in multiple disciplines of engineering, which is increasingly important in our technology-based society. However, existing robotics kits are mostly geared toward middle- and high- school students and either cost hundreds or thousands of dollars or have limited hands-on design capabilities. This leaves customizable robotics unaffordable to many schools, as well as neglects to introduce robots to impressionable elementary-age children. Our project focused on concurrently addressing three concerns: cost, age group, and creative potential. We developed a modifiable template for an affordable robot that students design themselves, supporting a project-based learning approach, with the goal of inspiring interest in STEM in kindergartners.

Since most robotics kits are cars, we designed a robotic boat and a web-based app, which students use to create and steer the boat. One boat is made of a flat sheet of plastic folded into a 3D structure, with basic electronics propelling the vehicle, and costs under \$40 total. In the app, powered by Robot Compiler technology, students change parameters on the boat to see the effect on the 2D printable template and 3D model of the finished boat. This focus on customization encourages iterative design and engages students firsthand in the engineering innovation process. Students have flexibility in designing their robots down to the component level, fostering a sense of ownership over their project and resulting in a more self-motivated learning experience.

Custom Printable Robotic Boats for Early STEM Education

Chelsea Lai, Shantinath Smyth, Dr. Ankur Mehta
 Dept. of Electrical and Computer Engineering, University of California, Los Angeles

Introduction

Problems with Existing Robotics Kits

Expensive

Middle- and high-school age group

Limited hands-on design

Our Solution

- Creating a design tool for low-cost foldable robotic boats

Educational Applications

- Students design, build, and redesign robotic boats
- Hands-on experience with cycle of scientific experimentation

Developing the Design Tool

Built prototypes of mechanically powered paddleboat design

→

Motorized boat and integrated electronics into design

→

Finalized boat template

→

Model 2D template and 3D structure on RoCo

Student Design Process

1 Design in web-based app by inputting parameters

2 Print and cut out template

3 Fold and assemble boat, Test effects of chosen parameters

Easily modify components

Results

- Iterative design process and customization allows for personalized products
- Encourages experimentation and hands-on learning approach
- Teaches gateway STEM skills and engineering/design process

Total cost: ~\$30 (Retail), ~\$15 (Bulk)

Ultra-thin Power Bank: \$13

Plastic film: <\$1

2 Continuous Rotation Servos: <\$10

NodeMCU board and Motorshield: \$6

Acknowledgements

Summer Undergraduate Research Program
 Fast Track to Success Program
 LEMUR Lab, Dr. Ankur Mehta
 Wireless Health Institute

References

[1] McLurkin, James, et al. "Using multi-robot systems for engineering education: Teaching and outreach with large numbers of an advanced, low-cost robot." IEEE transactions on education 56.1 (2012): 24-33.
 [2] Blumenfeld, Phyllis C., et al. "Motivating project-based learning: Sustaining the doing, supporting the learning." Educational psychologist 26.3-4 (1991): 369-398.
 [3] Rubenstein, Michael, et al. "eRobot: An affordable one-robot-per-student system for early robotics education." 2015 IEEE International Conference on Robotics and Automation (ICRA). IEEE, 2015.
 [4] Mondada, Francesco, et al. "The e-puck, a robot designed for education in engineering." Proceedings of the 9th conference on autonomous robot systems and competitions. Vol. 1. No. CONF. IPCB: Instituto Politecnico de Castelo Branco, 2009.
 [5] A.M. Mehta, J. DelPreto, B. Shaya, and D. Rus. "Cogeneration of Mechanical, Electrical, and Software Designs for Printable Robots from Structural Specifications". In: Intelligent Robots and Systems (IROS 2014), Chicago, IL, Sep 2014, pp. 2892-2897.
 [6] Mehta, Ankur M., and Daniela Rus. "An end-to-end system for designing mechanical structures for print-and-fold robots." 2014 IEEE International Conference on Robotics and Automation (ICRA). IEEE, 2014.

Prices of Existing Educational Robotics Kits

Robot	Retail Cost (USD)
Thymio	189
LEGO Mindstorm	340
Scribbler 3	199
mBot	69
Our Boat	30



LAB NAME
Speech Processing and Auditory Perception Laboratory

FACULTY ADVISOR
Professor Abeer Alwan

GRADUATE STUDENT DAILY LAB SUPERVISOR
Gary Yeung

DEPARTMENT
Electrical and Computer Engineering

Dan Song
Electrical Engineering
First Year
UCLA

Automated Speech Database Organization

The development of an autonomous social robot, able to deliver clinical and educational assessments to young children, has great potential to aid in the efforts of educators and help students reach age-appropriate levels of proficiency in reading and oral language skills. A study researching the feasibility of the JIBO robot for such purposes, as well as gathering data needed to improve child automated speech recognition (ASR), resulted in a large dataset of verbal interactions between the robot and children via the administration of the Goldman-Fristoe Test of Articulation (GFTA) and other language tasks. Prior to database publication, time consuming and error-prone tasks such as matching audio data with corresponding prompt-answer pairs and the notation of private information for removal must be performed. We present a design and Python implementation for software automating and simplifying such processes. As robot prompts are known and consistent, timestamps are detected in audio files using a cross-correlation approach. We propose several methods of avoiding computationally expensive operations during such a search. For files with transcripts, processing is done using both a brute force search and the SpaCy natural language processing package, the latter to identify possible private information. Results are compared and combined with those from audio processing. Finally, we propose a database organizational structure and documentation in preparation for future publication.



UCLA Samueli School of Engineering
Summer Undergraduate Research Program

Automated Speech Database Organization

Robert C. Ozturk¹, Dan Song¹, Gary Yeung¹ and Abeer Alwan¹

¹Department of Electrical and Computer Engineering, University of California, Los Angeles



Introduction



Figure 1. The JIBO personal assistant robot was released in November of 2017.

- What if a robot could help in the classroom?
- Recent research by Yeung et al. (2019) explored the feasibility of having the social robot JIBO (Figure 1) deliver educational assessments to young children [1].
- Additionally, data it produced was intended to be used towards developing better child automatic speech recognition (ASR), the current state of which has held back child human-robot interaction research [2].
- JIBO's administration of a letter and digit naming task and the 3rd Goldman Fristoe Tests of Articulation (GFTA-3) resulted in a large database containing 60 hours of child-robot interaction.
- This work presents an attempt to automate the necessary pre-processing of this database, as well as propose a database organizational structure.

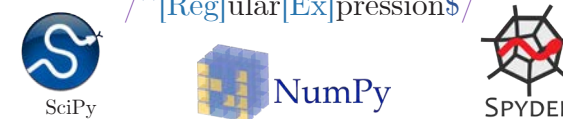
Database

- Subjects and Recordings:
- 156 children were recorded interacting with JIBO over 236 sessions.
 - Sessions lasted between 5 and 40 minutes.
 - Session length varied based on child engagement and experience.
 - Children were recorded in a classroom study space with limited noise.
- Tasks:
- 3rd Goldman Fristoe Tests of Articulation (GFTA-3)
 - Letter and digit naming task
- Transcriptions:
- Full transcripts of the audio were produced by trained transcribers.
 - Phonetic transcriptions were produced by trained phoneticians.

Objectives

- Create an easy to use interface for extracting/creating file information
- Automate the removal of private and sensitive data in audio
- Prepare database for publication and distribution for research

Methods



Design: Text Processing

- Processing of audio transcripts was utilized in multiple ways:
 - To extract task completion data for documentation
 - To identify private information
 - As a guiding tool when labeling and cutting audio
- Regular expression (regex) use on the predictable transcript layout allowed for such analysis.
 - Ex. “\((\d+:\d\d)\)” searches for timestamps of the form (min:sec)
- spaCy:
 - This open-source package for Natural Language Processing aided in identifying private information within files, decreasing manual work.
 - Part-of-Speech tagging and Named Entity Recognition (NER) were the two main features of the package utilized.

Design: Audio Processing

- Template-based recognition was used to perform time-delay estimation to find robot speech in an audio file (Figure 2). Results shown in Figure 3.

Figure 2. Flow-chart of template-based recognition

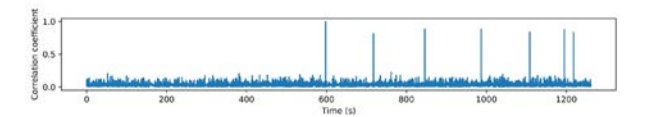
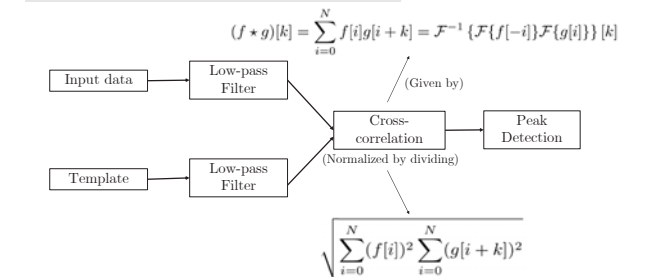


Figure 3. Results of one normalized cross-correlation. The large peaks are matches to some JIBO voice line. A vertical axis value of 1 indicates an exact match. Due to noise and microphone placement inconsistencies, an exact match was very rare and thresholding was used to determine whether a match took place.

Deliverables

- A new database layout was designed and accompanied with documentation using combined data from the designed processing methods.
- User interface was created for labeling and cutting audio. It decreases manual work by giving the user certain features:
 - Jump to audio containing private info or the beginning of certain tasks
 - Switch between textual and audio analysis (Figure 4) of child interviews

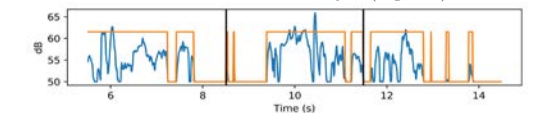


Figure 4. A small section of a sound file. The user selected section is between the two black vertical lines. The orange sound blocks can be snapped to while scrubbing or can be ignored if fine scrubbing is desired.

Conclusion and Future Work

- This database will assist in research for a number of diverse applications:
 - Child automatic speech recognition
 - Child speech science and linguistics
 - Human-robot interaction
- Going forward, we hope to generalize the methods for preliminary processing to all speech databases.

References

[1] Yeung, G., Afshan, A., Quintero, M., Martin, A., Spaulding, S., Park, H. W., ... and Alwan, A. (2019). Towards the development of personalized learning companion robots for early speech and language assessment. *2019 Annual Meeting of the American Educational Research Association (AERA)*.

[2] Yeung, G., & Alwan, A. (2018). On the Difficulties of Automatic Speech Recognition for Kindergarten-Aged Children. *Interspeech*, 1661–1665.

We would like to thank Professor Alwan, Gary Yeung, Amber Afshan, and Morgan Tinkler for the opportunity, guidance, and warm welcome given to us. Additional thanks to the UCLA Wireless Health Institute, UCLA ECE Fast Track Program, and the NSF for their continuing support, financially and otherwise, for undergraduate research.



LAB NAME
Communications Systems Laboratory

FACULTY ADVISOR
Professor Richard Wesel


GRADUATE STUDENT DAILY LAB SUPERVISOR
Ethan Liang


DEPARTMENT
Electrical and Computer Engineering

Wenhui Sui
Electrical Engineering
First Year
UCLA



Design of Cyclic Redundancy Check (CRC) for Tail-Biting Convolutional Codes

Reliable transmission of data requires channel codes that can correct errors introduced by the channel and/or detect that a received or decoded sequence is not valid. Convolutional encoders can correct errors in a distorted received sequence by using the Viterbi algorithm to find the closest convolutional codeword to the received sequence. Cyclic redundancy check (CRC) codes can detect whether the convolutional codeword identified by Viterbi decoding corresponds to a valid message. While both CRCs and convolutional codes have been developed in the past, they have been designed independently even though they are not independent when used together. For zero-terminated convolutional codes (ZTCCs) that are terminated by a final sequence of inputs that drives the encoder to the zero state, our research group has designed CRCs that are optimal for a given ZTCC. Tail-biting convolutional codes (TBCCs) avoid the overhead caused by ZTCCs and therefore can achieve higher rates with essentially the same performance. Rather than using additional input symbols to drive the final state to zero, TBCCs enforce the constraint that the starting state is the same as the final state. Our research is directed towards developing CRCs that are optimal for a given TBCC.





Design of Cyclic Redundancy Check (CRC) for Tail-Biting Convolutional Codes
 Vincent Lau¹, Wenhui Sui¹, Ethan Liang¹, Richard Wesel¹
¹Communications Systems Laboratory, Department of Electrical and Computer Engineering
 University of California, Los Angeles

Introduction

Reliable transmission of data requires channel codes that can correct errors introduced by the channel and/or detect that a received or decoded sequence is not valid. Convolutional encoders can correct errors in a distorted received sequence by using the Viterbi algorithm to find the closest convolutional codeword to the received sequence. We are particularly interested in the implementation of tail-biting convolutional codes (TBCC), which reduce overhead and are capable of achieving higher rates at practically no expense to performance. Cyclic redundancy check (CRC) codes can detect whether the convolutional codeword identified by Viterbi decoding corresponds to a valid message. While both CRCs and convolutional codes have been developed in the past, they have been designed independently even though they are not independent when used together. Our research is directed towards developing CRCs that are optimal for a given TBCC. By first implementing an encoder and decoder for convolutional codes, we are building towards designing CRCs to ultimately accomplish this goal.




Figure 1. Overall system structure of convolutional code and CRC for communications.

Convolutional Codes

Convolutional codes are error-correcting codes that rely on memory storage in encoding, distinguishing them from traditional linear block codes. The encoder employs a shift-register structure that utilizes delay blocks to compute the output and track the state. We focus on rate-1/n encoders, which take 1-bit inputs and produce n-bit outputs.

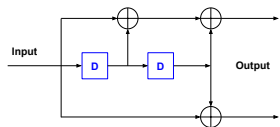


Figure 2. A convolutional encoder can be represented as a block diagram. The values inside the delay blocks (blue) represent the state of the encoder. [1]

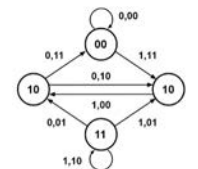


Figure 3. A state machine is used to determine the output for a particular input and state. It also shows the evolution of states in a compact way. [1]

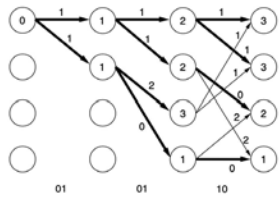


Figure 4. The Trellis diagram aids in keeping track of path metrics and surviving paths, which are utilized in Viterbi decoding. [1]

- The decoder we implement is based on the Viterbi algorithm, which can be realized with a Trellis diagram to keep track of the evolution of state paths over time, and helps us identify the most likely codeword given the received sequence.
- We are able to identify several performance metrics from the Trellis diagram, including free distance and number of nearest neighbors. The free distance represents the smallest Hamming distance between a pair of two valid codewords, while the number of nearest neighbors indicates the number of such pairs.
- While zero-terminated convolutional codes (ZTCCs) are terminated by a final sequence of inputs that drives the encoder to the zero state, tail-biting convolutional codes (TBCCs) require that the starting state be the same as the final state. These codes can achieve higher rates while maintaining nearly the same error-correcting performance.

Cyclic Redundancy Check (CRC)

Cyclic redundancy check (CRC) codes are error-detecting codes that help detect errors that may have been made by the decoder (e.g. the Viterbi decoder). At a high level, the CRC adds extra bits to the original codeword to serve as an extra layer of protection for decoding. This modification acts as an additional constraint to reduce the number of valid codewords, resulting in a smaller set of such valid codewords. This smaller set facilitates a larger minimum distance between codewords that provides a higher noise tolerance. In other words, the decoder will be less likely to select and validate an incorrect codeword.

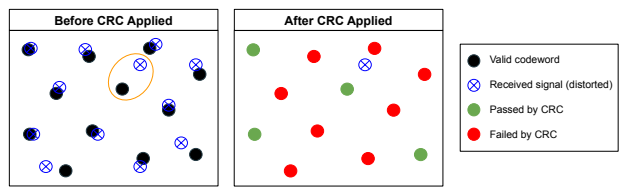


Figure 5. Visual representation of CRC operation: The figure at the left shows the space of valid codewords (black). Transmission over a channel creates noise, resulting in distortion in the received signals (blue). Sometimes the noise distorts the codewords so much that the decoder may associate the received signal with a different codeword (yellow), leading to an error in decoding. To limit this effect, the CRC will only pass specific codewords (green) and fail all others (red) to make the valid codewords distinct.

Materials and Methods

- This phase of the project primarily involved implementing a convolutional encoder and Viterbi decoder. This work was completed in MATLAB and was followed by extensive testing of both the codes and performance metrics for various examples of generator polynomials. We made sure to test different code rates and number of states.
- We started by simulating transmission across noiseless channels to make sure our encoder/decoder worked (i.e. zero errors occurred).
- For noisy channel transmission, we were interested in comparing bit-error rate (BER) vs. signal-to-noise ratio (Eb/No) for different rates and codes, as well as examining other properties like free distance, nearest neighbors, and analytic traceback depth.

Simulation Results

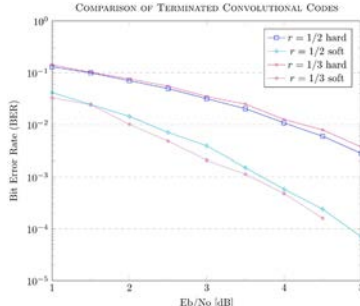


Figure 6. A performance comparison of bit-error rate (BER) vs. signal-to-noise ratio (Eb/No) between different generator polynomials for ZTCC. We tested codes with rate-1/2 and 1/3, which were decoded with both hard decision and soft decision.

- We compared two polynomials, (7,5) in purple and (13,12,16) in blue, which are of rate-1/2 rate-1/3, respectively.
- Two types of decoding were implemented and tested: hard-decision and soft-decision.
 - Hard-decision decoding uses a threshold value to decode a codeword.
 - Soft-decision decoding uses Euclidean distance to decode, which takes into account the impact of the noise on the transmission. Soft-decision decoding is the more refined and accurate technique of the two.
- As expected, the soft-decision decoding method outperformed the hard-decision decoding. Soft-decision required an Eb/No value about 2dB lower than hard-decision to produce the same BER.
- The rate-1/3 code performed better than the rate-1/2 code for soft-decision decoding, as expected. However, the two codes have similar performance for hard-decision decoding, which is an anomaly we are exploring (we expect the rate-1/3 to perform better).

Conclusions & Future Work

- Overall, our experience with the program was equal parts learning and re-implementing codes. We were able to develop a sound understanding of channel coding techniques and implement convolutional codes from scratch to supplement our learning process.
- For noiseless channels, we found that messages were decoded with zero error, as expected. Across noisy channels, noise was applied at different proportions, and we were also able to obtain good results (BER vs. Eb/No) for different parameters.
- We are looking towards the future to further develop our knowledge and bolster the significance of this project, with the ultimate goal of developing new CRCs for a range of CRC bit lengths. Specifically, we hope to eventually design new CRCs which are targeted for use with specific TBCCs, which we will implement.
- Our new CRCs will improve short-blocklength communications that are vital to sensor networks and the internet of things.

References

[1] R.D. Wesel, "Convolutional Codes", Wiley Encyclopedia of Telecommunications, John Wiley and Sons, 2003.
 [2] H.H. Ma, J.K. Wolf, "On Tail Biting Convolutional Codes", IEEE Transaction on Communications, 1986.
 [3] C.-Y. Lou, B. Daneshmand, R.D. Wesel, "Convolutional-Code-Specific CRC Code Design", IEEE Transactions on Communications, 2015.

Acknowledgments

We would like to thank the National Science Foundation and the Electrical and Computer Engineering Department for providing us the opportunity to conduct research. Additionally, we would like to acknowledge Ethan Liang and Hengjie Yang for providing guidance and mentorship throughout our research and learning process.



Madeline Taylor
Electrical Engineering
Second Year
UCLA

LAB NAME
Terahertz Electronics Laboratory

FACULTY ADVISOR
Professor Mona Jarrahi

GRADUATE STUDENT DAILY LAB SUPERVISOR
Dr. Nezih Yardimci and Deniz Turan




DEPARTMENT
Electrical and Computer Engineering

Optimization of Delay Stage of Terahertz Time-Domain Spectroscopy System


Terahertz time-domain spectroscopy (THz-TDS) allows us to analyze materials using pulses of terahertz radiation created by a femtosecond laser. Materials are analyzed based on their absorption patterns of the THz radiation. In the laboratory system, the detector receives pulses of THz radiation along with optical light pulses. The optical light path length is shifted by a delay stage which enables analysis of materials over a time domain and frequency domain.

Our goal is to miniaturize and improve the delay stage to convert the large laboratory system into a mobile, commercial device. The previous delay stage utilizes linear motion; a platform with mirrors accelerates back and forth to alter the path length of the radiation. Our main focus is designing a smaller prototype that relies on rotational acceleration to decrease the loss of speed from linear acceleration and deceleration.

Once a full prototype has been designed, it is tested in the laboratory setup and compared with previous data for accuracy. The frequency domain results of THz-TDS can be analyzed and used to determine chemical composition. When testing for accuracy, the Fourier graphs and THz pulses of our delay stage are directly compared with those of the laboratory stage. Our first test displayed broadening and shifting in the Fourier transformed waves which both indicate a worsened accuracy. However, the new delay stage works at almost double the frequency of the old one (2.2 Hz compared to 1.2 Hz) and only weighs 861 grams.

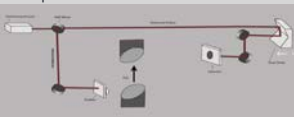
Optimization of Delay Stage of Terahertz Time-Domain Spectroscopy System



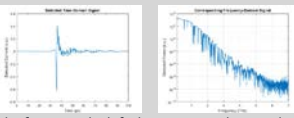
Background and Motivation

Terahertz Time-Domain Spectroscopy

- Allows analysis of chemical composition of materials using time-delayed pulses of terahertz radiation
- More efficient than prior methods because it is sensitive to amplitude and phase of radiation
- Materials and environments are analyzed based on their absorption patterns of the radiation
- Laboratory system utilizes a femtosecond laser source that produces electromagnetic radiation which follows two paths as depicted below



- One optical path passes through a terahertz emitter. The other is delayed by a mechanical stage to allow results to be made over a time domain
- Objects can be placed in the path of terahertz pulses for time-based spectroscopic analysis as shown below



The figure on the left shows one terahertz pulse detection over a time domain. Each dip and spike gives information that can be processed using Fourier analysis to create the figure on the right. The graph on the right gives detailed information about the material being analyzed over a frequency domain. In this case, the graph's dips show the water vapor content in the air since no specific object is being analyzed

Motivation

- Create a smaller, cost-efficient system for analyzing various materials specifically for agricultural, environmental purposes

Materials and Methods

Delay Stage

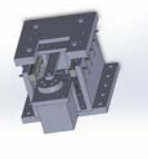
- DC motor powered by Arduino and H-bridge IC, L293D
- Initial prototypes of delay stage created by 3D printer with goals to outsource for final design

Prototype Designs

First Design:

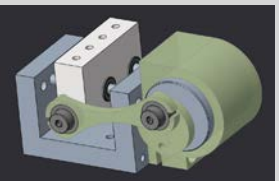
- Uses slider-crank mechanism to drive platform
- Powered by stepper motor

Frequency	2.2 Hz
Total Travel	2 cm
Weight	861 g
Size	18 cm x 12.2 cm x 8.9 cm
Price	about \$150



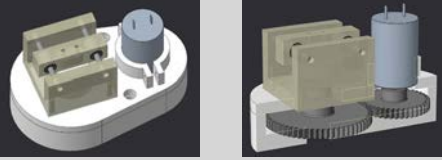
Second Design:

- Smaller slider-crank mechanism
- Powered by DC motor
- Much faster, but inconsistent speeds
- 101 grams (decrease in weight)



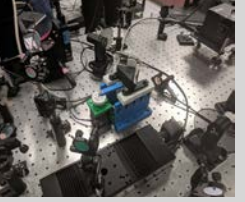
Third Design:

- Crank-inspired eccentric design
- Powered by DC motor and feedback system to stabilize speed (in progress)
- Greater inertia with the use of gears to drive the platform



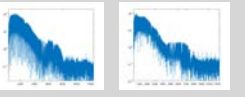
Testing and Results

We test our delay stage in the laboratory set up by aligning the mirrors to accurately reflect the laser beam on its path. We compare the pulses and Fourier transformed data using MATLAB to compare accuracy and efficiency.

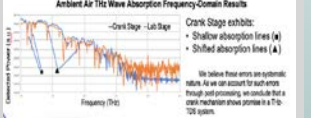


First design in laboratory setup

Results of First Design:




The Fourier transformed graphs of the first design's results (left) display a broadening in the dips compared to the standard results shown on the right. This depicts a decrease in accuracy.



The figure above shows our new data overlapping the data from the original laboratory delay stage. The shallow absorption lines and shifts in the absorption lines are indicated above. It shows promising results that also demonstrate a need for greater accuracy.

Current Work/Conclusion

We are currently improving each design by ordering new parts to improve stability and reciprocation. We are also implementing a PID feedback system using a proximity sensor to increase reliability and control. A crank mechanism presents promising results for use in the actuation of a THz-TDS delay stage so we hope to continue improving on accuracy and speed with this next design shown to the right.



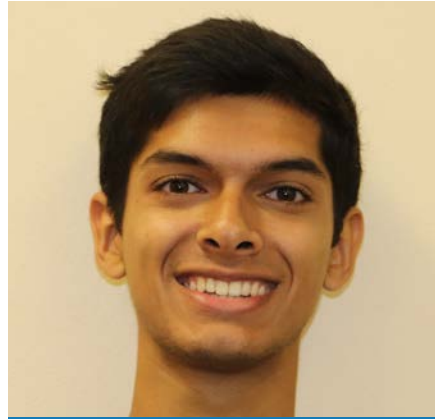
	Second Design	Third Design	In Progress Design
Frequency (Hz)	N/A ¹	10.4	N/A ²
Total Travel (cm)	1.2	0.7	1.1
Weight (g)	101	211	N/A ²
Size (cm ³)	7.4 x 6.6 x 4.6	9.4 x 6.2 x 5.4	
Price	\$220	\$260	\$300

¹ Frequency instability makes this value nonessential
² N/A statistics have not been measured due to work in progress

This table compares the second and third design in the two left columns. The third column design is currently in progress.

Acknowledgements

This work was supported by the National Science Foundation through the UCLA Summer Undergraduate Research Program organized by William Herrera.



LAB NAME
Neptune Laser Laboratory

FACULTY ADVISOR
Professor Chan Joshi

GRADUATE STUDENT DAILY LAB SUPERVISOR
Daniel Matteo

DEPARTMENT
Electrical and Computer Engineering

Ravi Varma
Electrical Engineering
First Year
UCLA

Sub-micrometer Precision Optical Delay Stage for Synchronization of Ultrafast Laser Pulse

As laser systems produce shorter and shorter pulses to push the limits of ultrafast and high field science, the requirements for precision timing and optical synchronization in the lab have increased accordingly. The coordination and control of the relative time delay between ultrafast pump and probe laser pulses is required to resolve short lived physical events. Time and space are intimately connected for light, and on picosecond and femtosecond time scales, errors and uncertainties in the optical path length on the order of micrometers and nanometers can drastically degrade the time resolution of measurements in the laboratory. We have implemented an optical delay stage powered by a DC servo motor and controlled by a LabVIEW program. To evaluate the accuracy of positioning two laser pulses, we study the stage's accuracy and repeatability in creating an optical path length delay with a HeNe laser Michelson interferometer. The pointing stability and reproducibility of the spatial beam profile after the stage is also determined. Understanding of the stage's precision will enable us to perform picosecond pump-probe experiments, or synchronize ultrafast laser pulses using cross-correlation.

Sub-micrometer Precision Optical Delay Stage for Synchronization of Ultrafast Laser Pulse

Ravi Varma, Daniel Matteo, Sergei Tochitsky, Chan Joshi
Neptune Laboratory
Department of Electrical and Computer Engineering
University of California, Los Angeles

Introduction and Motivation

- In order to resolve ultrafast events, synchronization of short laser pulses is crucial
 - As pulses become shorter, optical systems must become more accurate and stable to ensure correct measurements
- Synchronization of such pulses will result in more accurate pump-probe experiments
- Pump-Probe: One intense pulse interacts with the experimental sample while the weak probe pulse is affected by the interaction
 - Used to study laser-matter interactions in many fields including plasma physics, femtochemistry, and condensed matter physics

Methods

- We assembled a delay stage, translated by a DC motor, which can control the optical path length of the probe pulse relative to the pump pulse
- A LabVIEW program controls the motor and collects data from an oscilloscope in either single shot or continuous shot modes
- We move the delay stage back and forth repeatedly to measure the pointing stability of a CW Helium-Neon (HeNe) laser beam ($\lambda = 632.8 \text{ nm}$)
 - We measure stability by tracking the beam's centroid on a CCD camera
- We then set up Michelson interferometer using a HeNe laser to distinguish the stage's positional precision
 - We track movement of the fringes across the CCD

Interferometry

- Using the wave nature of light to extract phase information from overlapped beams
 - Once combined, constructively interfering parts of the beam will produce bright fringes and destructively interfering parts will produce dark fringes
 - We use a beam splitter to split the HeNe laser into two paths
 - Light traveling along those paths are reflected back by mirrors, one static and one dynamic, its position controlled by the delay stage (Michelson Interferometer)
 - Movement of our delay stage changes the relative phase of the two interfering beams

Pointing Stability Experimental Setup

Distribution of the Beam positions after translating the delay stage in either μm or mm steps

Positions of Beam about 30mm with 1 μm steps and 1 mm steps

Plotting Trends of X and Y displacements of beam starting from 30mm vs actuator position

- For 1 μm steps, the system jitters, but is reproducible within 40 μrad
- For 1mm steps, the system is reproducible, but systematic mechanical errors begin to arise, and the beam starts to drift significantly in the vertical direction

- Integrate full image to get fringe intensity, which should vary with a period of 632.8 nm path length delay (orange curve)
- Over 8 μm of stage movement, we accumulate approximately 700 nm of error from our expected path length delay

- By measuring the position of fringes, we determined the total accumulated phase at each stage position, and thus the true position of the stage
- We relate this to the time delay via the speed of light, and find that for every 8 μm we accumulate an error of 3 fs

Conclusion

- We find that our delay stage gives us a pointing stability of 25 μrad within μm steps, but increases to 50 μrad at mm steps
 - Stability is worse the farther away the stage is from its origin
- Using interferometric techniques, we determined that:
 - For every 8 μm , we accumulate 700 nm of translational error or about 3 fs of time delay error
 - Movement in the forward direction is reliable, whereas movement backwards is inconsistent
- We demonstrated the optical delay stage's ability to synchronize ultrafast laser pulses on sub-picosecond time scales

References

- A. J. Alcock and P. B. Corkum, Can. J. Phys., 57, 1280
- Introduction to Optics, "Chapter 11." by Frank L. Pedrotti and Leno S. Pedrotti, Prentice Hall, 1993.



LAB NAME
Sensors and Technology Laboratory

FACULTY ADVISOR
Professor Robert Candler



GRADUATE STUDENT DAILY LAB SUPERVISOR
Jimmy Wu

DEPARTMENT
Electrical and Computer Engineering

Sydney Walsh
Electrical Engineering
Second Year
UCLA



Millimeter-Scale Magnetic Shielding

Devices that rely on atomic spectroscopy, such as nuclear magnetic resonance gyroscopes and atomic clocks, are strongly affected by external magnetic fields. Thus, in order to miniaturize these devices while maintaining precision, small-scale magnetic shields must be developed to properly redirect magnetic field lines away from the enclosed devices. The purpose of our research is to fabricate and test potential shield designs. Based on previous research, we determined that the optimal design would consist of concentric cylinders of alternating high permeability and low permeability material. By alternating layers, we partially prevented adjacent ferromagnetic material from reducing the magnetization of that layer. Moreover, multilayer shielding allowed us to mitigate the effects of magnetic saturation, as a single layer of magnetic material would reach saturation more quickly, limiting the shield's ability to generate an opposing field. We conducted our research by simulating potential shield designs in COMSOL Multiphysics, developing an appropriate test setup to assess the effectiveness of our shields, and fabricating shields to test. For our test setup, we generated a magnetic field using an electromagnet and measured the magnetic flux density using a printed circuit board with a magnetometer mounted at its tip; shielding factor was determined by taking the ratio of external to internal magnetic field. Shields were fabricated by electroplating alternating layers of permalloy and copper.

Millimeter-Scale Magnetic Shielding

Sydney Walsh, Hou Seng Wong, Justin Shao, Jimmy Wu, Robert Candler
Department of Electrical and Computer Engineering, University of California, Los Angeles

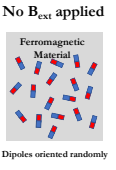



Purpose

- Devices that rely on atomic spectroscopy (atomic clocks, NMR gyroscopes, etc.) are sensitive to external magnetic fields
- In order to miniaturize these devices while maintaining precision, we must enclose them in small-scale magnetic shields
- Our research serves primarily to test and fabricate potential shield designs

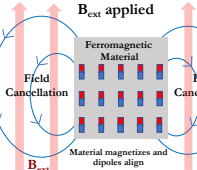
Magnetic Shielding Overview

No B_{ext} applied



Dipoles oriented randomly

B_{ext} applied



Material magnetizes and dipoles align

- Shields created from high permeability ferromagnetic material
- When an external magnetic field (B_{ext}) is applied, the previously randomly ordered dipoles align in the direction of the applied field, generating an opposing magnetic field
- These fields cancel, redirecting B_{ext} away from the device enclosed in the shield
- Magnetic material reaches saturation when a strong enough external magnetic field is applied that the material cannot magnetize further, decreasing effectiveness of shielding

Shield Design

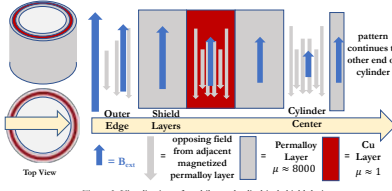


Figure 3: Visualization of multilayered cylindrical shield design.

- Concentric cylinders of alternating high permeability and low permeability material
- Magnitude of external magnetic field decreases each successive layer with max shielding in the center
- Alternating material prevents adjacent layers of ferromagnetic material from demagnetizing each other
- Having multiple layers mitigates effects of saturation

Methods

Test Setup




Figure 4: Photos of test setup.

- External magnetic field generated by electromagnet with current outputted by function generator
- Magnetic flux density inside (B_{int}) and outside (B_{ext}) the shield measured by printed circuit board with magnetometer mounted at its tip
- We perform 2 trials: one increasing the magnetic field without the shield (B_{ext}) and another with the shield (B_{int})
- Shielding Factor: $S = B_{ext}/B_{int}$

Fabrication

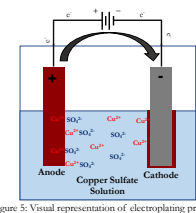


Figure 5: Visual representation of electroplating process.

- Electroplate alternating layers of permalloy and copper onto cylindrical wax mold and then dissolve wax in xylene solution
- To electroplate permalloy, use nickel and iron as anode instead of copper

Results & Discussion

COMSOL Simulations for Multilayer Cylinder

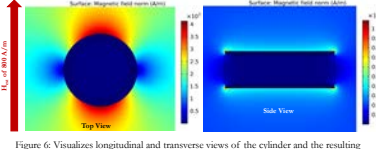



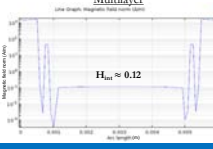
Figure 6: Visualizes longitudinal and transverse views of the cylinder and the resulting magnetic field norm. Illustrates the effectiveness of this design, as the magnetic field norm drastically decreases within the cylinder.

Single Layer



$H_{int} \approx 1.2$

Multilayer



$H_{int} \approx 0.12$

Figure 7: Comparison between multilayer and single layer cylindrical shields of same material, dimensions, and thickness in order to assess the effectiveness of multilayered shielding. Charts depict magnetic field norm in a line through the center of the cylinder in the direction of the applied magnetic field. The results prove that multilayer designs are more effective than single layer designs before saturation, as shielding factor for the multilayer shield is considerably larger for cylinders of the same dimensions, material, and external magnetic field.

Plate vs. Cylinder Design

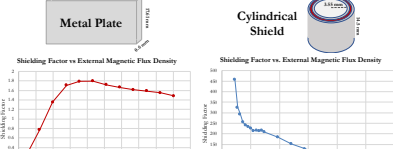


Figure 8: Results collected from our test setup for cylindrical and metal plate shield designs.

- Cylindrical shield: alternating permalloy and copper layers
- Metal plate shield: single permalloy layer
- Cylindrical design observed to have higher shielding factors overall
- Shielding factors appear to decrease as materials approach saturation
- Metal plate B_{int} seems to have linear relationship with B_{ext} , while for the cylinder, the rate B_{int} increases is much less than that of B_{ext}
- B_{int} of permalloy plate seems to increase at a similar rate to B_{ext} , while for the cylinder, the rate B_{int} increases is much less than that of B_{ext}

Plate vs. Cylinder Mapping

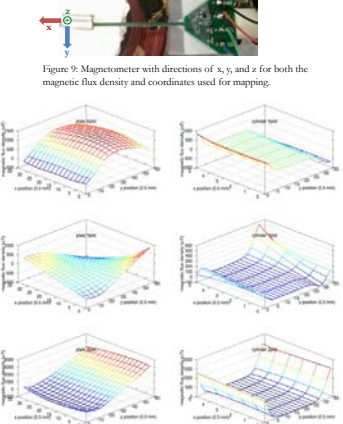


Figure 9: Graphs of magnetic flux density (in x, y, z directions) relative to position on cylindrical and metal plate shields.

Conclusion and Future Work

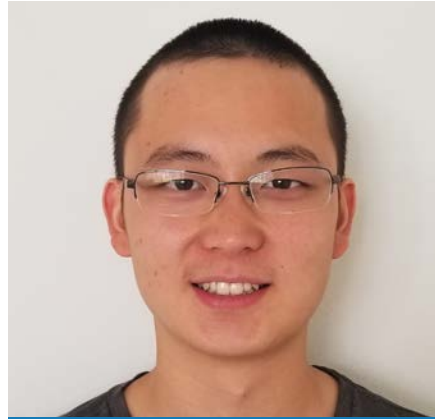
- Our simulation and test setup results imply that our multilayer, cylindrical design provides more optimal shielding than the commonly used plate design
 - COMSOL simulations confirmed that alternating layers of high and low permeability material produced a higher shielding factor than a single layer of the same thickness, inner radius, and material
 - By applying different magnetic fields and measuring B_{int} and B_{ext} , we found that our cylindrical design had higher shielding factors overall and that B_{int} increased at a much slower rate when increasing B_{ext} compared to the plate design
- In the future, we plan on testing and fabricating more shields of different geometries and examining the possibility of electroplating metal directly onto devices

References

- [1] Donley E., Hodby, E., Hollberg, L., and Kitching, J. Demonstration of high-performance compact magnetic shields for chip-scale atomic devices. 2007.
- [2] Dubay, L., NIST scientists win 2014 Rank Prizes for chip-scale atomic clock. 2013.
- [3] Hodges, E., Millimeter-Scale Electroplated Conformal Magnetic Shields. 2018.
- [4] Wu, J., Li, L., Harrison, J., and Candler, R. Micro- to Millimeter Scale Magnetic Shielding. 2017.

Acknowledgements

I would like to thank the Sensors and Technology Laboratory for having me in their lab, the National Science Foundation and Functional Nanomaterials Summer Scholars Program for funding my research, and the UCLA SURP program for giving me this unique opportunity.



LAB NAME
Communications Systems Laboratory

FACULTY ADVISOR
Professor Richard Wesel

GRADUATE STUDENT DAILY LAB SUPERVISOR
Ethan Liang

DEPARTMENT
Electrical and Computer Engineering

Derek Xiao
Electrical Engineering
Third Year
UCLA

Computing Channel Capacity using the Blahut-Arimoto Algorithm

The maximum rate at which information can be reliably transmitted over a communication channel is the channel capacity, usually represented in units of bits per channel use. The ability to compute the capacity of any discrete memoryless channel based on its statistical description is a powerful and fundamental result of information theory. Broadly speaking, the noisier a channel, the lower its capacity.

Mathematically, the channel capacity is the maximum mutual information between the input and output of the channel, where the maximum is taken over possible input distributions. My research is focused on developing tools to identify the mutual-information-maximizing input distribution for a channel and consequently its capacity. As an initial project, I have implemented the Blahut-Arimoto algorithm, which finds the capacity-achieving distribution for any discrete memoryless channel with a finite input alphabet.

For many practical channels, the input alphabet is not finite. For example, even a simple amplitude shift keying system has an uncountably infinite number of possible amplitudes. Furthermore, there are practical communication systems where the optimal input distribution turns out to be asymmetric, such as on-off keying over an additive white Gaussian noise channel. My future research is directed towards identifying the optimal input distributions in these cases and developing practical encoders that can approximate those optimal input distributions.

Computing Channel Capacity Using the Blahut-Arimoto Algorithm



Derek Xiao, Ethan Liang, Prof. Richard D. Wesel
Department of Electrical and Computer Engineering
University of California, Los Angeles



Motivation

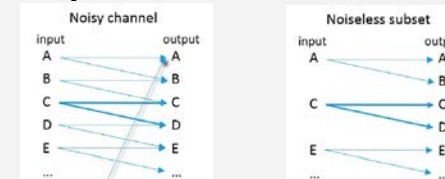
In our communication technology, whether it's TV or satellite communications, the fundamental goal is to **send bits with low power and low error**. This initial project is focused on finding the highest rate at which information can be transmitted with **zero error**, the channel capacity. Since analytic derivation of the capacity is sometimes unfeasible, I implement an iterative algorithm that can find the optimal input distribution, and consequently the capacity.



What is Channel Capacity?

Definition
- **Channel Capacity**: The maximum information rate (in bits per transmission) at which information can be transmitted reliably (with no error) through a noisy channel.

Example
- noisy typewriter channel
- Capacity: $\log_2(26/2)$, achieved by using only half of the inputs



Some Intuition
- *noisier* typewriter channel (n equiprobable outputs given an input)
- Capacity: $\log_2(26/n)$, achieved by using only $1/n$ of the inputs.
- *noisier channels have a lower capacity*

What is Mutual information?

- **mutual information**: measurement of how much information X and Y share. how much knowing one of the variables reduces uncertainty about the other.

Examples
- X = dice roll, Y = indicator of whether the roll is even or odd
- $I(X;Y) = 1$ (bit)
- X = dice roll, Y = a different, independent dice roll
- $I(X;Y) = 0$ (bits)



Computation of Channel Capacity

$$C = \max_{p(x)} I(X; Y)$$

C = channel capacity
p(x) = input probability distribution
I(X;Y) = mutual information between X and Y
X, Y = random variables

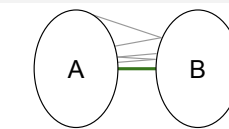
- It turns out that mutual information, $I(X;Y)$, is convex over the possible input distributions, $p(x)$, allowing for application of convex optimization techniques.
- I implement the **Blahut-Arimoto algorithm** to solve for capacity of a few example channels.

Acknowledgements

We would like to thank the UCLA ECE Fast Track to Success Program, NSF Summer Undergraduate Research Program for their financial support, and for this opportunity to explore research.

What is the Blahut-Arimoto Algorithm?

Projection on Convex Sets (POCS)

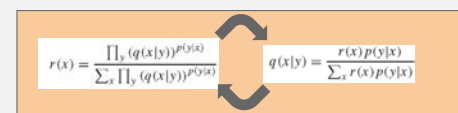


- we can find the minimum distance between two convex sets by randomly picking a $x \in A$ and finding the closest $y \in B$, then repeating until convergence.

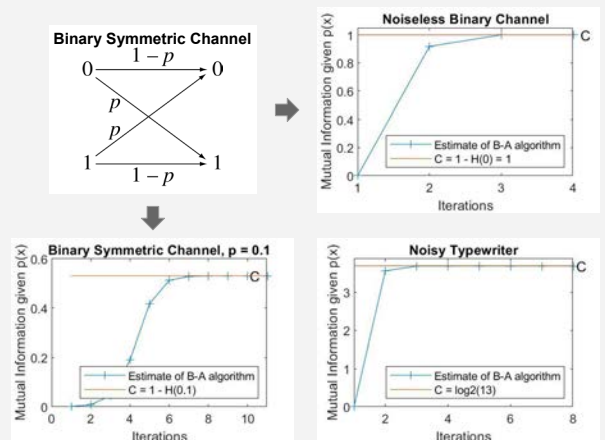
$$d_{\min} = \min_{a \in A, b \in B} d(a, b)$$

$$C = \max_{p(x)} \max_{q(y)} \sum_x \sum_y r(x) p(x) \log \frac{q(y|x)}{r(x)}$$

- it turns out that $I(X;Y)$ is a distance which satisfies the right properties, and we can write the capacity maximization expression in the form of a POCS problem, so we apply the iterative procedure described above.



Results



Conclusions and Future Work

All results converge to the correct theoretical values, validating my implementation of the Blahut-Arimoto algorithm.
My implementation works for discrete memoryless channels with a finite input alphabet. However, for many practical channels, the input alphabet is not finite. For example, even a simple amplitude shift keying system has an uncountably infinite number of possible amplitudes.
My future research is directed towards identifying the optimal input distributions in these cases and developing practical encoders that can approximate those optimal input distributions.
My immediate next project is to find the optimal input distribution given any average power constraint on an on-off keying channel with additive Gaussian noise.



If you would like to find out more about the Summer Undergraduate Research Program,
please contact Director William Herrera:

William Herrera

Director

Undergraduate Research Program

310.825.9478

williamh@seas.ucla.edu

Engineering Student Resource Center, 6288 Boelter Hall

Or visit our website at <https://tinyurl.com/uclasurp>.